https://doi.org/10.5194/egusphere-2026-5589
Preprint. Discussion started: 24 September 2026

Beyond rainfall thresholds: hydrologic controls on debris-flow initiation in alpine channels

Markus Hrachowitz[1], Roland Kaitna[2]

[1]Department of Water Management, Faculty of Civil Engineering and Geosciences, Delft University of Technology, Stevinweg 1, 2628CN Delft, Netherlands
[2]Institute of Mountain Risk Engineering, BOKU University, Vienna, Austria

Correspondence to: Markus Hrachowitz (m.hrachowitz@tudelft.nl)

Abstract.
Debris flows are a severe natural hazard in mountain regions. As a spatially and temporally highly irregular phenomenon, meaningful quantitative description and generalization of the underlying processes in contrasting environments as well as associated robust local prediction of debris flows is hindered by a lack of sufficiently detailed observations. As a consequence, debris flows are frequently predicted based on simple regional precipitation (or rainfall) intensity-duration thresholds that lump many channels over larger spatial domains, irrespective of potentially different underlying debris flow trigger processes due to hydro-climatic or geomorphic differences between the channels. Based on long-term debris flow records of up to 18 years, hydro-climatic observations and modelled hydrological variables across three contrasting active debris flow channels (ID1-ID3) in the Austrian Alps, this study (1) analyses differences between the local debris flow regimes in these channels, based on their strength of temporal coupling with hydro-climatic and hydrological extremes, (2) quantifies differences between regional and local debris flow initiation thresholds that emerge from these differences in their temporal coupling, and (3) identifies the pairs of threshold model variables that allow the most reliable debris flow predictions in each of the three study channels. We have found that the three study channels are characterized by considerable difference in seasonal debris flow timing. In channel ID1, debris flows events are largely confined to early summer, occurring, on average, several weeks before the wettest conditions in each year, thus being only weakly coupled to hydro-meteorological extremes. In the close-by channel ID2, debris flows occur throughout summer, on average a few days after the wettest conditions of any specific year. The high debris flow frequency in this channel in addition suggests multiple cycles of sediment exhaustion and re-supply to the channel over one season. Together, this is evidence for a stronger coupling and a highly dynamic balance between the availabilities of sufficient sediment and in-stream transport capacity, respectively. Due to the geographical proximity of and thus similar hydro-climatic conditions in ID1 and ID2, the differences in debris flow regimes can largely be attributed to differences in landscape characteristics and thus geomorphic predisposition. In contrast, in channel ID3, debris flows are largely confined to late summer and temporally coincide with the wettest annual conditions, suggesting a strongly coupled debris flow regime. The differences between ID3 and the other channels arise from the combined influence of hydro-climatic and geomorphic

https://doi.org/10.5194/egusphere-2026-5589
Preprint. Discussion started: 24 September 2026

predisposition. These differences in debris flow regimes are reflected in the differences between the individual local thresholds across the three channels and the systematically superior performance of local thresholds to detect debris flows than regional thresholds across all channels. It was further found that traditional precipitation and rainfall thresholds were consistently outperformed by thresholds that explicitly account for the sum of rainfall and snowmelt. The overall strongest thresholds were found to be the ones based on channel discharge, providing a direct descriptor of in-stream transport capacity. Together the results provide evidence for the benefit of local thresholds and explicitly accounting for hydrological variables in threshold-based debris flow prediction models.

https://doi.org/10.5194/egusphere-2026-5589
Preprint. Discussion started: 24 September 2026

1 Introduction

Debris flows are fast flowing, multi-phase mixtures of water and sediment that surge down steep channels (Hungr et al., 2014; Brenna et al., 2020). As major natural hazards in mountainous regions they cause every year numerous human casualties, disruption and economic damage world-wide (Dowling and Santi, 2014). The detailed physical trigger mechanisms of debris flows are not yet fully understood and remain subject of ongoing debate. However, there is broad consensus that their occurrence is, next to geomorphological properties (e.g. Moreno et el., 2025) and similar to shallow landslides (Mirus et al., 2025), linked to precipitation intensities and volumes and thus also to the resulting subsurface water storage and magnitude of stream flow (e.g. Takahashi, 1978; Gregoretti and Dalla Fontana, 2008; Kean et al., 2013; Bennet et al., 2014; Bogaard and Greco, 2018; Palucis et al., 2018; Prenner et al., 2018; Bernard et al., 2025). Theoretical and empirical evidence suggests that climate-change leads, amongst other factors, to increases of precipitation intensities and associated river flood peaks (e.g. Haslinger et al., 2025; Astagneau et al., 2026). As a consequence, it therefore needs to be expected that occurrence frequencies and magnitudes of debris flows will likewise be affected (e.g. Hirschberg et al., 2021; Kaitna et al., 2023a; 2025), emphasizing the need for reliable prediction models.

Typically, debris flows are temporally sharply confined and spatially highly localized events in steep mountain watersheds. Depending, amongst others, on channel geometry and flow rate, the time between a debris flow being triggered and the sediment eventually being re-deposited further downstream does in many cases not exceed a few minutes. Debris flows can thus be characterized by much shorter timescales than slower and more gradually moving landslides. In addition, they also occur at smaller spatial scales. Debris flows are not only often initiated from diffusely defined sediment source areas whose location in or close to stream channels can be highly variable over time, but debris flows also remain spatially largely confined to these channels when propagating downwards. As such, debris flows are controlled by the local interplay between the manifold and complex processes of sediment supply from varying source area locations and in-stream transport capacity (Montgomery and Buffington, 1997; Palucis et al., 2018).

Together the above characteristics of debris flows pose major observational obstacles because it is problematic to anticipate in which (parts of a) channel debris flows may occur and where initiation source areas are located at any given moment. This is further exacerbated by the relatively low frequency of debris flow occurrence in specific individual channels, which rarely exceeds 10 individual debris flow events per year and is commonly much lower. As a consequence, there are world-wide only a few intensely monitored natural channels with data for a sufficiently large sample of recorded historical debris flow events in combination with spatially and temporally high-resolution concomitant long-term data of hydrometeorological variables. This lack of data has so far limited our ability to generalize the physical mechanisms that lead to the initiation of debris flows beyond the few monitored channels and thus to generalize parametrizations of process-based models (Bennet et al., 2014; Gregoretti et al., 2016; McGuire et al., 2017). In contrast, data-driven approaches to describe debris flow initiation, mostly based on precipitation intensity-duration thresholds are less data-intensive (e.g Guzzetti et al., 2008; Berti et al., 2012; Bel et al., 2017; Kaitna et al., 2025). However, the relative scarcity of debris flows, incomplete event documentation, and comparably

https://doi.org/10.5194/egusphere-2026-5589
Preprint. Discussion started: 24 September 2026

short observation time series of frequently <10 years in many channels imposes another set of limitations: to allow sufficiently large debris flow samples for meaningful statistical analysis, these models are almost exclusively implemented at larger, regional scales, aggregating debris flow data from many different channels. Such regional threshold models have in the past proven useful to identify time periods with hydrometeorological conditions with increased debris flow occurrence probability over larger spatial domains. The major disadvantage is that the use of spatially lumped regional thresholds does not allow to predict where, i.e. in which channel or in which catchment within the spatial domain debris flows may be expected to occur. Correspondingly, little is known about general differences in debris flow regimes, e.g. supply- vs. transport-limited, between channels, as well as about differences in initiation thresholds in different channels.

Overall, this implies that debris flows remain problematic to reliably predict in time and space. As a step towards closing this knowledge gap, the objectives of this study, based on up to 18 years of documented debris flows and hourly hydro-meteorological data in three contrasting debris flow-active channels in high alpine terrain in Austria, are (1) to analyze and describe the differences between the local debris flow regimes in these channels based on their strength of temporal coupling with hydro-climatic and hydrological extremes, (2) to quantify differences between regional and local debris flow initiation thresholds that emerge from these differences in their temporal coupling as well as (3) to identify the pairs of threshold model variables that allow the most reliable local debris flow predictions in each of the three channels.

2 Study area

This study is based on data from three small, hydro-meteorologically and physiographically distinct high-elevation catchments along the alpine main ridge in Austria. All three study catchments are characterized by rather frequent debris flow occurrence. Detailed catchment characteristics are provided in Figure 1 and Table 1.

Briefly, the Hopfgartnergraben catchment (ID1c; Fig.1a-c, Fig.2a), with an area of 2.29 km^2 and a mean elevation of 1993 m a.s.l., is a side valley of the Defereggen valley and features mostly south-facing, steep hillsides with a mean slope of i ~ 0.86. The channel network itself is characterized by a somewhat milder mean slope of i_c ~ 0.53. The lower elevation parts of the catchment are mostly spruce forest, with a total areal fraction A_f = 0.16, and grassland (A_g = 0.09). In contrast, higher elevations are mostly covered by shallow-rooted, high alpine vegetation (A_h = 0.54) or are largely unvegetated (A_u = 0.21). Throughout the catchment, loam soils dominate, underlain by metamorphic lithology of mostly highly erodible micaschist formations. The mean annual precipitation in the catchment is ~1150 mm yr^{-1}. With a mean annual temperature of 3˚C, ~39% of precipitation, on average, falls as snow, leading to the presence of a seasonal snowpack typically from end of October until beginning of June. During the observation period, debris flows observed in the catchment are exclusively triggered from higher elevation parts of the central channel with well-defined and documented source areas that supply the channel with sediment (Fig.2d). The most downstream point of the source areas delimits the sub-catchment area that affects debris flow initiation (0.72 km^2; ID1) and which is used for the subsequent analysis of debris flow occurrence and trigger thresholds. While characterized by the same soil textures and lithology, this debris flow initiation area sub-catchment (ID1) has, in contrast to the overall

https://doi.org/10.5194/egusphere-2026-5589
Preprint. Discussion started: 24 September 2026

catchment (ID1c), a higher mean elevation of 2211 m a.s.l., moderately steeper slopes ($i \sim 0.97$, $i_c \sim 0.67$) and less abundant vegetation with a large fraction unvegetated ($A_u = 0.27$) or covered by high-alpine vegetation ($A_h = 0.71$).

The Loechertroggraben catchment (ID2c; Fig.1d-f; Fig.2b) is also located in the Defereggen valley, ~7 km west of the Hopfgartnergraben (ID1c). It has an area of 0.3 km^2, a mean elevation of 1789 m a.s.l. and features mostly steep, north-facing, shaded terrain with a mean slope of $i \sim 0.86$ and a similarly steep channel system ($i_c \sim 0.71$). Wide parts of the catchment are covered by spruce and larch forest ($A_f = 0.73$), with a large, contiguous patch of unvegetated scree debris ($A_u = 0.23$) below a sharp escarpment in the centre of the catchment. Soils with loam texture dominate throughout the catchment. Orthogneiss in the lower part and unsorted moraine material in the upper part with patches of highly erodible Phyllonite along the edges of the escarpment characterize the geology of the catchment. The catchment has a mean annual temperature of 4.7˚C and receives ~1160 mm yr^{-1} precipitation, around 44% of which falling as snow. Seasonal snowpacks are typically present between early November and end of May. Sediment is supplied to the channel mostly from the unvegetated scree debris patch and the episodically collapsing escarpment above. The downstream end of this source area therefore defines the sub-catchment ID2, in which past debris flows were initiated (Fig.2e). This sub-catchment ID2 has a mean elevation of 1912 m a.s.l and is characterized by slightly gentler terrain slopes ($i \sim 0.7$) but a steeper channel ($i_c \sim 0.77$) than the overall catchment. A third of ID2 is covered by unvegetated scree ($A_u = 0.33$) and most of the remainder with forest ($A_f = 0.63$).

Table 1. Hydro-climatic characteristics and landscape properties of the study catchments.

	Hopfgartnergraben		Loechertroggraben		Lattenbach	
	catchment	source area	catchment	source area	catchment	source area
ID	ID1c	ID1	ID2c	ID2	ID3c	ID3
Location outlet	46˚55’23” N 12˚31’18” E	46˚55’56” N 12˚30’59” E	46˚55’00” N 12˚25’03” E	46˚54’44” N 12˚25’05” E	47˚08’07” N 10˚30’45” E	47˚08’56” N 10˚30’01” E
Period debris flow observations	2005-2022		2020-2022		2005-2022	
Number observed debris flow events	12		24		17	
Mean annual temperature T [˚C]	3.0	1.7*	4.7	4.0*	4.0	3.5*
Mean annual precipitation P [mm yr^{-1}]	1150	1150	1160	1160	1010	1010
Mean annual fraction of P falling as snow [-]**	0.39	0.45	0.44	0.46	0.38	0.42
Mean annual potential evaporation E_P [mm yr^{-1}]	570	540	340	330	710	690
Mean annual stream flow Q [mm yr^{-1}]**	710	715	930	930	520	525
Long-term mean runoff ratio $C_R = Q/P$ [-]**	0.61	0.62	0.80	0.80	0.51	0.52
Catchment area A [km^2]	2.29	0.72	0.30	0.13	5.41	2.28
Elevation range [m]	1127-2728	1592-2656	1340-2067	1676-2067	833-2968	1158-2729
Mean elevation [m]	1993	2211	1789	1912	1740	1830
Mean catchment slope i [-]	0.86	0.97	0.86	0.70	0.78	0.76
Mean channel slope i_c [-]	0.53	0.67	0.71	0.77	0.31	0.33
Areal fraction forest A_f [-]	0.16	0.02	0.73	0.63	0.23	0.16
Areal fraction grass A_g [-]	0.09	0.00	0.00	0.00	0.06	0.00
Areal fraction high alpine vegetation A_h [-]	0.54	0.71	0.04	0.04	0.35	0.45
Areal fraction unvegetated/bare rock A_u [-]	0.21	0.27	0.23	0.33	0.36	0.39
Soil texture†	Loam		Loam		Loam	
Lithology‡	Micaschist		Orthogneiss		Limestone/Micaschist	

*estimates based on environmental lapse rate of 0.006˚Cm^{-1}; **estimates from hydrological model; †from https://soilgrids.org/ (last access 30/01/2026; Poggio et al., 2021); ‡from https://maps.europe-geology.eu (last access 30/01/2026; Hollis et al., 2022)

https://doi.org/10.5194/egusphere-2026-5589
Preprint. Discussion started: 24 September 2026

The Lattenbach catchment (ID3c; Fig.1g-i; Fig.2c) drains in south-east direction into the Sanna river. It has an area of 5.4 km^2 and a mean elevation of 1740 m a.s.l. While the hillsides are very steep (i ~ 0.78), the channel network in the valley bottoms follows milder gradients (i_c ~ 0.31). The catchment is covered by deciduous-dominated forest (A_f = 0.23) at lower elevations and high-alpine vegetation (A_h = 0.35) and unvegetated (A_u = 0.36) parts at higher elevations. Soils are typically of loam texture. The catchment is located along a fault line between micaschist formations of the crystalline and the northern calcareous Alps, characterized by deep-seated mass movements within the heavily stressed bedrock. Mean annual temperature reaches 4°C and precipitation ~1010 mm yr^{-1}, around 38% of which on average falls as snow. Seasonal snowpack is typically present between end of October and early June. Debris flows have in the past exclusively been initiated in the southern-most channel (Fig.2f). Sediment of the weathered weak bedrock and post glacial deposits are fed into the channel by deep-seated landslides at movement rates up several meters per year (Aigner et al., 2023). The most downstream point of these source areas delimits the sub-catchment area that is associated with debris flow initiation (2.28 km^2; ID3). At a mean elevation of 1830 m a.s.l., the debris flow initiation sub-catchment (ID3) features similar characteristics than the overall catchment (ID3), with comparable terrain and channel slopes and a dominance of high-alpine vegetation (A_h = 0.45) and unvegetated surfaces (A_u = 0.39).

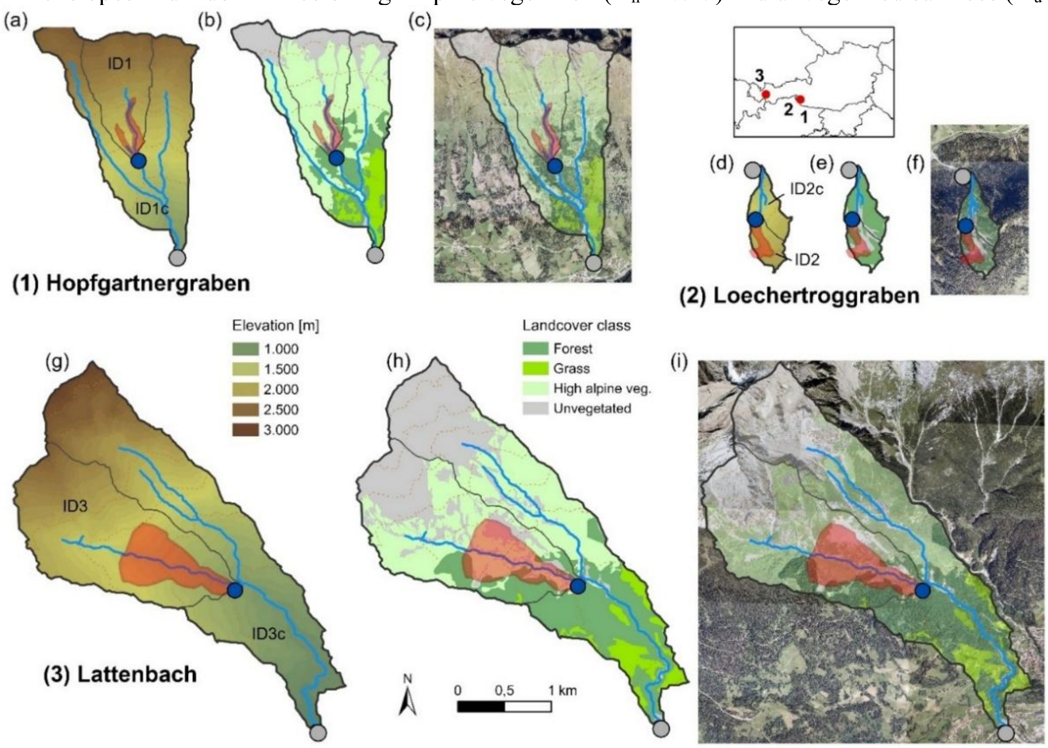

Figure 1. Elevation and landcover, as well as orthophotos overlain by landcover for the three study catchments: (a)-(c) Hopfgartnergraben, (d)-(f) Loechertroggraben and (g)-(i) Lattenbach. The grey circle symbols indicate the outlets of the overall catchments (ID1c, ID2c and ID3c). The blue circle symbols indicate the outlets of the sub-catchments in which observed debris flows were initiated (ID1, ID2, ID3). The red shaded areas indicate the locations of documented sediment source areas. The small context map (Source: ©EuroGeographics, EBM v2020), shows the locations of the three study catchments in Austria

https://doi.org/10.5194/egusphere-2026-5589
Preprint. Discussion started: 24 September 2026

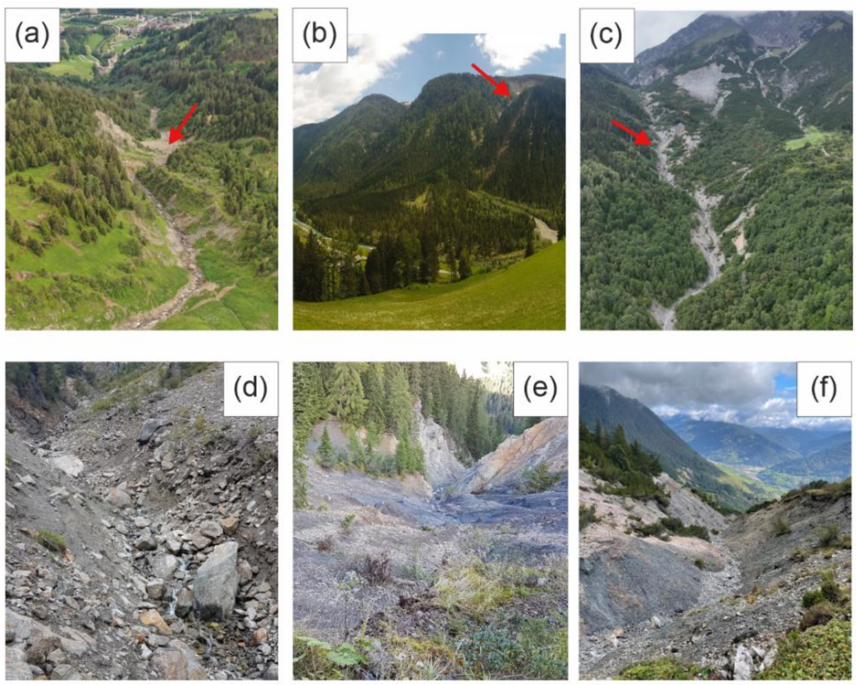

Figure 2. Photos of the three study catchments (a) ID1c – Hopfgartnergraben, (b) ID2c – Loechertroggraben and (c) ID3c – Lattenbach. The red arrows indicate the location of photos of the channels source areas in (d) ID1 – Hopfgartnergraben, (e) ID2 – Loechertroggraben and (f) ID3 – Lattenbach.

3 Data

3.1 Debris flow data

Debris flow event data in the Hopfgartnergraben catchment (ID1c) were available through an inventory of documented debris flows, managed by the Austrian Ministry of Agriculture and Forestry, Climate and Environmental Protection, Regions and Water Management (BMLUK, 2026) for monitoring periods 2005-2022 and completed by an automatic digital camera, located at the outlet of the catchment, at a 10-minute time interval for the period 2020-2022. In total 12 debris flow events were observed in the catchment during the 18-year monitoring period, i.e. on average ~0.67 yr^{-1} (Fig.3a). In most years, a maximum of one single debris flow occurred, with the exception of 2021, when three debris flows occurred. Data from detailed field surveys following the debris flows (Wagner, 2022; Kaitna et al., 2023b.) suggest that all events were initiated within a narrowly defined source area that supplied the sediment by physical weathering of the adjacent bedrock outcrops (ID1; Fig.1a-c, Fig. 2d). Due to the lack of active landslides or substantial amounts of quaternary deposits along the channel, we geomorphologically classify ID1 as supply-limited catchment (Bovis & Jakob, 1999; Hirschberg et al., 2022; Qui et al., 2024).

Due to the lack of elements at risk in the vicinity of the Loechertroggraben catchment (ID2c) , information on past debris flow activity in the public inventory is, in contrast to ID1c, limited. For this study, debris flow events in ID2c were exclusively observed by two automatic cameras, installed at the outlet of ID2c, with a 10-minute recording timestep. Observations are available between 2020 and 2022. Due to harsh environmental conditions and logistical constraints, the operation of the camera was restricted to the summer period between end of May and mid-October. Throughout the 3-year monitoring campaign, a total of 24 debris flows was observed with an average of 8 yr^{-1} (Fig.3b). Based on detailed field evidence (Bernardi, 2022; Kaitna et al., 2023b) it was found that all observed debris flows were initiated at the distal reach of an unvegetated, steep and instable scree patch, where all water and eroded sediment is funnelled into a narrow bedrock gorge (ID2; Fig.1d-f, Fig.2e). The rather high sediment-supply rate from this active source area is expected to be responsible for the exceptional debris flow activity during the observation period and is reflected in a prominent depositional fan at the outlet of the catchment.

At the Lattenbach catchment (ID3c), the occurrence and flow dynamics of debris flows are systematically monitored by the Institute of Mountain Risk Engineering at BOKU University (Huebl and Kaitna, 2021), providing a complete dataset for the 2005 – 2022 period. During this 18-year period a total of 17 debris flow events were recorded (Fig.3c). The number of events per year range from none to a maximum of three, with an average of ~0.95 yr^{-1}. In contrast to the two other catchments, field surveys and remote sensing suggest that debris flows are mostly initiated along a channel reach, where deep-seated landslides continuously supply sediment to the channel (ID3; Fig.1g-I, Fig.2f).

3.2 Hydrometeorological and hydrological data

Hourly mean catchment precipitation (P) and temperature (T) were obtained from the 1x1 km^2 gridded INCA reanalysis product operated by GeoSphere Austria (Haiden et al., 2011) for the three study catchments over the 2005 – 2022 study period. Minor gaps in the data series were filled using observations from the nearby weather stations Hopfgarten (for ID1, 2) and See im Paznaun (for ID3) operated by the regional Hydrographic Services (HD Tirol; ehyd.gv.at; last access 30/01/26). Hourly potential evaporation E_P was estimated based on the method proposed by Hargreaves and Samani (1982). For the 2020-2022 period stream water-level observations were available at 10-minute intervals through the wildcameras installed at the catchment outlets. From these observations average hourly water levels H_{est} (cm) were visually and semi-quantitatively classified into 2 cm intervals, similar to Clerc-Schwarzenbach et al. (2025). Despite uncertainties involved, this nevertheless allowed overall distinction between general flow magnitudes and the timing of their occurrence. In addition, direct in-situ stream flow measurements Q_o (m^3s^{-1}) were available for several days in the study catchments.

Gridded snow cover information was obtained for the 2005-2022 study period for the three study catchments from the remotely sensed MODIS/Terra MOD10A1 product that provides daily retrievals of Normalized Difference Snow Index NDSI at a spatial resolution of 500m (Hall and Riggs, 2016). All available daily images from January 2005 to December 2022 were used in the analysis.

https://doi.org/10.5194/egusphere-2026-5589
Preprint. Discussion started: 24 September 2026

3.3 Preprocessing of MODIS, detection of snow cover and estimation of snow line elevation

The MODIS snow cover data had to be pre-processed to produce elevation dependent time series of daily snow cover presence for each of the three study catchments similar to what is described by Parajka and Blöschl (2008). Briefly, each catchment was stratified into 250m elevation bands. The presence of snow cover in each elevation band for each time step was then detected based on the Normalized Difference Snow Index (NDSI). Following Tong et al. (2020) and given the characteristics of the study catchments, MODIS cells with NDSI ≥ 0.3 were flagged as snow covered. If the fraction of cloud free MODIS cells within an elevation band was ≥ 0.1 and the mean NDSI of these cells ≥ 0.3, the entire elevation band *m* was labelled as "snow" ($s_{O,m,i}$=1) for that time step *i*. Conversely, if the fraction of cloud free cells within an elevation band was < 0.25 and the mean NDSI of these cells < 0.3, the entire elevation band was labelled as "no snow" ($s_{O,m,i}$=0) for that time step. If, due to cloud cover neither of these cases were met, the elevation band was labelled as "unknown" ($s_{O,m,i}$=NaN) for that time step *i*. This resulted, for each elevation band *m*, in binary a time series of observed "snow" ($s_{O,m,i}$=1), "no snow" ($s_{O,m,i}$=0) or "unknown" ($s_{O,m,i}$=NaN), which were further used for model calibration as described in Section 4.1. For visualization, the daily time series of snow line elevation E_{SL} (m), i.e. the lowest elevation band in which snow was detected at any time step *i* ($s_{O,m,i}$=1), was determined for each catchment over the study period. In case one or more elevation bands were cloud covered ($s_{O,m,i}$=NaN) on a specific day, a lower and upper potential limit of E_{SL} was determined from the lowest and the highest elevation bands that were not cloud covered on that day. Due to cloud cover, observed snow information was available on $\overline{N_{S_O}} \sim 145\ d\ yr^{-1}$, on average across the three catchments over the study period.

https://doi.org/10.5194/egusphere-2026-5589
Preprint. Discussion started: 24 September 2026

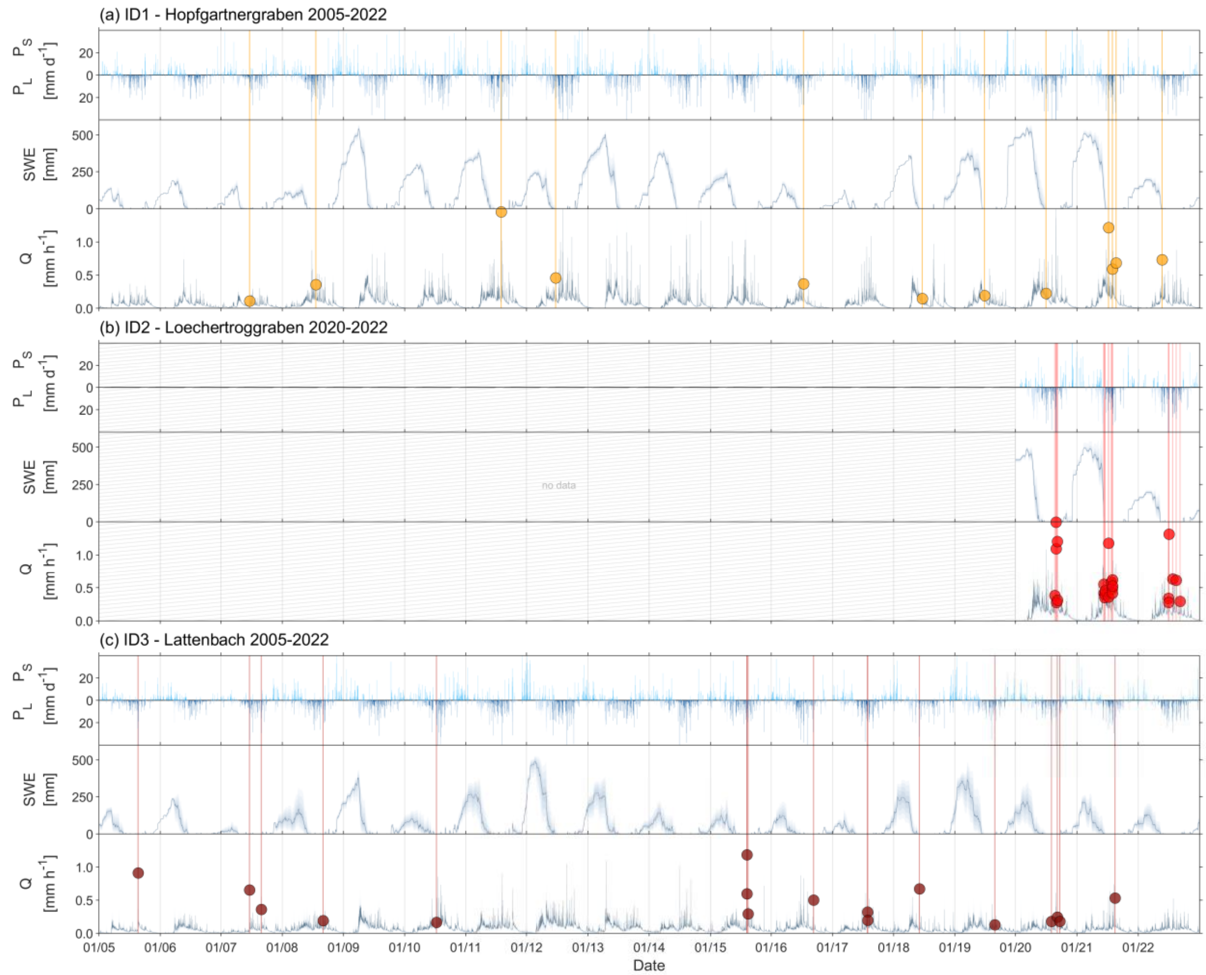

Figure 3. Time series of observed debris flows events together with hydrometeorological and hydrological variables for the (a) Hopfgartnergraben (ID1), (b) Loechertroggraben (ID2) and (c) Lattenbach (sub-)catchments (ID3). The orange, light red and dark red bars indicate the date of observed debris flows and the circle symbols indicate the channel discharge Q associated with each debris flow. The top rows of each panel show daily snowfall P_S (light blue bars), as well as liquid water input P_L as a sum of snow melt (light grey bars) and rainfall (dark blue bars). The middle rows show modelled snow water equivalent SWE and the bottom rows modelled discharge Q. The light shaded areas indicate the 5/95th uncertainty interval of SWE and Q. Note, the modelled variables are here shown for the reader to provide better context. Detailed descriptions of the hydrological model are provided hereafter in section 4.1 and detailed model results are provided in section 5.1.

https://doi.org/10.5194/egusphere-2026-5589
Preprint. Discussion started: 24 September 2026

4 Methods

The subsequent experiment involves four steps: (1) calibration of the hydrological model at the outlets of the three study catchments (ID1c-3c; Figure 1), (2) re-run the models for the debris flow initiation sub-catchments (ID1-3; Figure 1) with rescaled elevation and landcover type distributions but without further re-calibration, (3) readout time-series of modelled variables rainfall P_R, liquid precipitation P_L (rainfall plus snow melt), relative soil moisture S_U and stream flow Q and (4) estimate two dimensional regional and local thresholds for debris flow initiation based on these variables.

4.1 Hydrological model

4.1.1 Model architecture

A semi-distributed, process-based model is used to reproduce the hydrological dynamics of the study catchments. The model is based on the modular modelling framework described by Prenner et al. (2018), with similar successful implementations in the region (Hanus et al., 2021; Ponds et al., 2025) and elsewhere (Nijzink et al., 2016; Hulsman et al., 2021; Bouaziz et al., 2022; Tempel et al., 2024; Wang et al., 2024). All model equations are given in Supplementary Material Table S1.
Briefly, each catchment is discretized into K = 4 distinct hydrological response units (HRUs), representing the land cover classes “forest”, “grassland”, “high alpine” and “unvegetated” (Figures 1, 4). Each HRU is further stratified into 250m elevation bands. The aim is to allow for some heterogeneity in the representation of dominant physical processes while limiting model complexity (Euser et al., 2015).

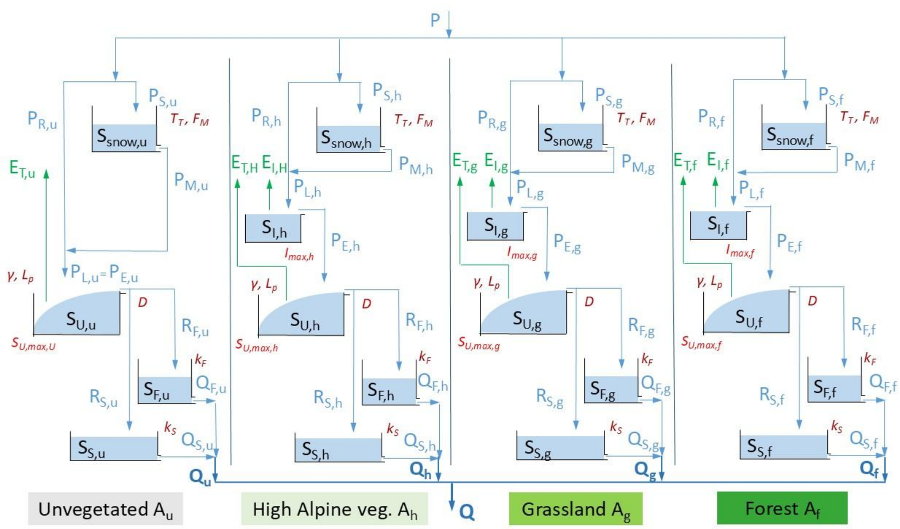

Figure 4. Semi-distributed model architecture, discretized into four parallel HRUs, each representing one of the four landcover types in the study catchments. Boxes represent storage components, red symbols represent model parameters and light blue symbols represent intern model fluxes. Fluxes that are released from the model are represented by darker blue (streamflow) and green symbols (evaporative fluxes).

https://doi.org/10.5194/egusphere-2026-5589
Preprint. Discussion started: 24 September 2026

More specifically, for each elevation band m in each HRU k the temperature is estimated from catchment mean $\overline{T}(t)$ and the elevation dependent environmental lapse rate according to $T_{k,m}(t) = \overline{T}(t) - 0.006^{\circ}Cm^{-1}$. Depending on $T_{k,m}(t)$ and the threshold temperature T_T, a model calibration parameter, precipitation P(t) is then either falling as snow $P_{S,k,m}(t)$ and stored in $S_{snow,k,m}(t)$ of a specific elevation band in a HRU, or entering the system as rainfall $P_{R,k,m}(t)$. If at a given time step $T_{k,m}(t)>T_T$, water is released from the snow storage $S_{snow,k,m}(t)$ as snowmelt $P_{M,k,m}(t)$, regulated by a parameter representing the snow melt factor F_M. At each time step, the liquid precipitation $P_{L,k}(t)$ that enters each HRU is then estimated as the sum of rainfall and snowmelt from each elevation band, weighted by the respective areal fractions $f_{k,m}$ of the individual M elevation bands:

$$P_{L,k}(t) = \sum_{m=1}^{M} f_{k,m} \left(P_{R,k,m}(t) + P_{M,k,m}(t)\right) \qquad \text{(Eq.1)}$$

Note that snow accumulation and melt dynamics, e.g. volume of water stored as snow $S_{snow,k,m}(t)$ or snow melt $P_{M,k,m}(t)$, vary between the K individual HRUs due to different elevations distributions (Figure 1) and thus temperatures $T_{k,m}(t)$.

$P_{L,k}(t)$ in each individual HRU then enters the interception storage $S_{I,k}(t)$ of that HRU, from where it is either released as evaporation $E_{I,k}(t)$ or, if it exceeds the interception storage capacity $I_{max,k}$, as effective liquid precipitation $P_{E,k}(t)$, which eventually reaches the subsurface and enters the unsaturated rootzone $S_{U,k}(t)$ as soil moisture. The rootzone $S_{U,k}(t)$ in each HRU is represented by a rootzone storage capacity parameter ($S_{U,max,k}$), a vegetation water stress parameter (L_p), a non-linearity parameter (γ) and a splitter (D). Together these parameters control the release of water from $S_{U,k}(t)$ along three pathways: as vegetation transpiration $E_{T,k}(t)$, as percolation $R_{F,k}(t)$ into a fast responding, lateral preferential flow network $S_{F,k}(t)$, from where it is released as $Q_{F,k}(t)$ or as groundwater recharge $R_{S,k}(t)$ into $S_{S,k}(t)$ from where it is released as groundwater flow $Q_{S,k}(t)$ so that the total water volume released from each HRU to the stream at each time step is $Q_k(t) = Q_{F,k}(t) + Q_{S,k}(t)$.

The total catchment stream flow Q(t) is then estimated as the sum of the outflows from the K individual HRUs $Q_k(t)$, weighted by the respective areal fractions A_k of the individual HRUs (Table 1):

$$Q(t) = \sum_{k=1}^{K} A_k Q_k(t) \qquad \text{(Eq.2)}$$

Catchment totals of all other variables are equivalently determined by areal weighting their values according to the areal fractions of the HRUs. For the variables total catchment rainfall $P_R(t)$, liquid precipitation $P_L(t)$, and soil moisture $S_U(t)$ used in the subsequent threshold analysis this was formulated as:

$$P_R(t) = \sum_{k=1}^{K} A_k P_{R,k}(t) \qquad \text{(Eq.3)}$$

$$P_L(t) = \sum_{k=1}^{K} A_k P_{L,k}(t) \qquad \text{(Eq.4)}$$

$$S_U(t) = \sum_{k=1}^{K} A_k S_{U,k}(t) \qquad \text{(Eq.5)}$$

https://doi.org/10.5194/egusphere-2026-5589
Preprint. Discussion started: 24 September 2026

4.1.2 Model implementation and calibration

The model was run on an hourly time step for the period 2005-2022 (ID1c, ID3c) and 2020-2022 (ID2c), with an additional six-month warm-up preceding these periods. In total, the model features 14 parameters, two of which are fixed. The 12 remaining calibration parameters include seven global parameters that are the same for each HRU and five vegetation related parameters that vary between the HRUs (Table 2).

The model was individually calibrated for the study catchments (ID1c-ID3c) to simultaneously reproduce three aspects of the hydrological response, following a multi-criteria calibration strategy to ensure a robust representation of model internal dynamics (e.g. Gupta et al., 2008; Efstratiadis and Koutsoyiannis, 2010; Hrachowitz et al., 2014). More specifically, the first calibration criterion was the presence of snow cover. If over a 24-hour period the maximum modelled snow storage in elevation band *m* was $S_{snow,m} \geq 0.5$ mm, that modelled elevation band for that day *i* was labelled as "snow" ($s_{M,m,i}$=1) otherwise as "no snow" ($s_{M,m,i}$=0). From that the areally weighted average fraction of days with correctly predicted presence of snow cover E_{SC} across all *M* elevation bands was, similar to Tong et al. (2021), calculated as:

$$E_{SC} = 1 - \sum_{m=1}^{M} f_m \frac{\sum_{i=1}^{N_{so,m}} |s_{M,m,i} - s_{O,m,i}|}{N_{so,m}} \quad \text{(Eq.6)}$$

where $s_{O,m,i}$ is the observed occurrence of snow on day *i* (see section 3.3), $s_{,M,m,i}$ is the modelled occurrence of snow on day *i*, $N_{So,m}$ is the total number of non-cloud-covered observation days in each elevation band *m*, i.e. with $s_{O,m,i}$=1 or 0, and f_m is the areal fraction of each elevation band.

The above was complemented by the Nash-Sutcliffe efficiency of hourly stream flow $E_{NS,Q}$ and the squared Spearman Rank correlation R^2_{WL} between observed hourly water level classes and modelled hourly stream flow, as suggested by Clerc-Schwarzenbach et al. (2025). While $E_{NS,Q}$ serves as a constraint on flow magnitudes, the non-parametric R^2_{WL} is a constraint on the timing of flow. As it is based on ranks rather than absolute magnitudes, it is not influenced by the non-linear water level – stream flow relationship and thus serves as constraint on the monotonic relationship between water level and stream flow.

In a Monte-Carlo approach with 10^6 realizations the uninformed prior parameter distributions (Table 2) were sampled. For each realization, the overall combined model performance with respect to all three calibration criteria was calculated as the Euclidean Distance to the "perfect model", i.e. D_E=0 (e.g. Schoups et al., 2005; Hrachowitz et al., 2014, 2021):

$$D_E = \sqrt{\frac{1}{3}(1 - E_{SC})^2 + \frac{1}{3}\left(1 - E_{NS,Q}\right)^2 + \frac{1}{3}(1 - R^2{}_{WL})^2} \quad \text{(Eq.7)}$$

The 2500 parameter combinations with the lowest D_E were retained as behavioural solutions and used for the subsequent analysis. To construct the parameter posterior distributions and the associated uncertainty intervals of the modelled variables, the retained solutions were weighted using a likelihood measure $L = D_E^{ß}$, with exponent ß=2 (cf. Freer et al., 1996).

https://doi.org/10.5194/egusphere-2026-5589
Preprint. Discussion started: 24 September 2026

Note that due to the lack of stream observations for the Lattenbach catchment (ID3c), the parameters were sampled from the combined posterior distributions of the Hopfgartnergraben (ID1c) and Loechertrog catchments (ID2c) and then exclusively calibrated against E_{SC}. This was deemed feasible as the posterior parameter distributions of ID1c and ID2c widely overlapped with each other and also closely resembled those of other close by catchments (e.g. Prenner et al., 2018; Hanus et al., 2021; Ponds et al., 2025), indicating broadly similar hydrological properties and functioning across the wider region.

As dictated by data availability, the model was calibrated towards E_{SC} using 2/3 of the years of available snow observations (i.e. 2011-2022 for ID1c, ID3c; 2021-2022 for ID2c) while $E_{NS,Q}$ and R^2_{WL} were limited to data from 2021. The models were tested based on E_{SC} for the remaining 1/3 of snow observations not used for calibration (i.e. 2005-2010 for ID1c, ID3c; 2020 for ID2c).

For further analysis, the model was re-scaled and run for the sub-catchments associated with the debris flow initiation areas (ID1, 2, 3) using the 2500 retained parameter sets, and by adjusting the areal fractions A_k of the four HRUs as well as their elevation distributions from the ones used for the calibration catchments (i.e. ID1c, 2c, 3c) to the ones of the sub-catchments (ID1, 2, 3) without any further re-calibration as similarly demonstrated by Gao et al. (2016). To account for uncertainties arising from limited observations, the analysis is based on the 5/95th uncertainty intervals of the modelled variables obtained from the retained parameter sets.

Table 2. Model prior and posterior parameter distributions and performance metrics for the three study catchments. The parameter and performance metric values shown are the values associated with the best performing model, i.e. lowest D_E, and the 5/95th uncertainty interval of all retained solutions (in brackets).

			Hopfgartnergraben (ID1c)	Loechertroggraben (ID2c)	Lattenbach (ID3c)
	Parameter	Prior distribution	Posterior distribution	Posterior distribution	Posterior distribution**
Global	T_T [°C]	-5-10	1.9 (0.7-2.7)	6.6 (3.4-8.9)	0.9 (-0.85-5.4)
	F_M [mm hr^{-1} °C^{-1}]	0.01-0.50	0.11 (0.09-0.30)	0.32 (0.14-0.40)	0.09 (0.07-0.47)
	D [-]	0-1	0.25 (0.12-0.37)	0.15 (0.13-0.58)	0.24 (0.12-0.37)
	k_F [hr^{-1}]	0.01-0.40	0.09 (0.04-0.28)	0.24 (0.03-0.32)	0.05 (0.05-0.28)
	k_S [hr^{-1}]	0.001-0.005	0.002 (0.001-0.002)	0.002 (0.001-0.002)	0.002 (0.001-0.003)
	L_p [-]	0.05-0.95	0.91 (0.30-0.92)	0.68 (0.29-0.91)	0.52 (0.30-0.92)
	γ [-]	0.25-2.00	1.69 (0.59-1.70)	1.23 (0.56-1.69)	1.55 (0.58-1.69)
Unvegetated	$S_{U,max,U}$ [mm]	0-20	16 (6-19)	10 (3-19)	17 (5-19)
High Alpine	$I_{max,h}$ [mm]	1.0*	1.0	1.0	1.0
	$S_{U,max,h}$ [mm]	10-50	20 (20-48)	33 (22-47)	42 (21-49)
Grassland	$I_{max,g}$ [mm]	0.5*	0.5	0.5	0.5
	$S_{U,max,g}$ [mm]	25-125	99 (52-97)	90 (53-97)	97 (51-98)
Forest	$I_{max,f}$ [mm]	1.5-3.0	2.4 (2.1-2.9)	2.6 (2.1-2.9)	2.8 (2.0-2.9)
	$S_{U,max,f}$ [mm]	100-300	166 (132-265)	190 (110-288)	171 (131-264)
	Performance metric				
Calibration	E_{SC}†		0.88 (0.86-0.94)	0.95 (0.89-0.97)	0.94 (0.86-0.93)
	$E_{NS,Q}$††		0.87 (0.71-0.89)	0.77 (0.42-0.72)	-
	R^2_{WL}††		0.49 (0.36-0.49)	0.75 (0.52-0.76)	-
Evaluation	E_{SC}‡		0.92 (0.89-0.96)	0.91 (0.82-0.94)	0.93 (0.87-0.93)

*fixed parameter; **for ID3c sampled from the combined posterior distributions of ID1c and ID2c; †calibration period ID1c, ID3c: 2011-2022, ID2c: 2021-2022; ††ID1c, ID2c: 2021; ‡evaluation period ID1c, ID3c: 2005-2010, ID2c: 2020

https://doi.org/10.5194/egusphere-2026-5589
Preprint. Discussion started: 24 September 2026

4.2 Debris flow initiation threshold models

4.2.1 Threshold model types

Here we use two-dimensional threshold models in the general form of $y = \alpha x^{\beta}$ as suggested by Caine (1980) and following the interpretation of Marra et al. (2025). Next to frequently used precipitation (P) and rainfall (P_R) duration-intensity thresholds, i.e. P_d-P_i and $P_{R,d}$-$P_{R,i}$ (e.g. Borga et al., 2005; Guzzetti et al., 2008; Berti et al., 2012; Jakob et al., 2012; Zhuang et al., 2015; Bel et al., 2017; Leonarduzzi et al., 2017; Jiang et al., 2021; Kaitna et al., 2025), also thresholds based on several other combinations of variables were tested. Although snow melt P_M can play a considerable role for debris flow initiation in snow dominated regions (e.g Mostbauer et al., 2018; Prenner et al., 2018), it has rarely been explicitly accounted for in threshold models, with one exception being Meyer et al. (2012). We here therefore included duration-intensity thresholds of modelled liquid precipitation P_L as a sum of rainfall and snowmelt (P_L=P_R+P_M), i.e. $P_{L,d}$-$P_{L,i}$. Similarly, the roles of soil moisture S_U, as manifestation of antecedent wetness (e.g Prenner et al., 2019; Long et al., 2020; Kaitna et al., 2023a), and stream flow Q (Kean et al., 2013; Wei et al., 2017; Bernard et al., 2025), as expression of the aggregated hydrological response, for the initiation of debris flows are increasingly acknowledged. This has motivated the use of these modelled variables in combination with P_L intensity to test the following three further threshold relationships, S_U-$P_{L,i}$, Q-$P_{L,i}$ as well as Q-S_U. Note that the variables P_R, P_L, S_U and Q were extracted from the models that were rescaled to the sub-catchments ID1, ID2 and ID3, associated with the debris flow initiation areas in the three study catchments.

The thresholds were established based on hourly (cf. Marra, 2019) pairs of variables with mean intensities over the preceding event duration, whereby events were defined as time spells of P, P_R and P_L, respectively, > 0 mm hr^{-1} and not interrupted by dry periods exceeding 6 hours.

The vast majority of previous studies has developed lumped thresholds over sets of multiple channels and spatial domains that can sometimes extend to over several thousand square kilometres. While the effects of spatial structure of precipitation fields on lumped debris flow thresholds over such large areas have been studied (e.g. Destro et al., 2017; Marra et al. 2017), the sensitivity of thresholds to specific physical properties of individual channels only starts to be explored (e.g. Moreno et al., 2025). To evaluate the difference of thresholds between individual channels and the effect of using lumped thresholds we here develop separate thresholds for the three individual study channels ID1, ID2 and ID2, hereafter referred to as “local thresholds” as well as lumped thresholds, from the combined data of all three study channels, hereafter referred to as “regional thresholds”

4.2.2 Determination and evaluation of initiation thresholds

The parameters α and ß of the individual debris flow initiation thresholds were randomly sampled 10.000 times from uniform prior distributions $0.01 \leq \alpha < 10$ and $0.0001 \leq ß < 2$. From these 10.000 realizations, the thresholds with the parameter combination that maximizes the balanced accuracy bAcc were retained as optimal solutions. This metric is defined as the average between the true positive rate R_{TP} = TP/P (number of correctly predicted debris flow events – true positives – TP over

https://doi.org/10.5194/egusphere-2026-5589
Preprint. Discussion started: 24 September 2026

the total number of debris flow events P) and the true negative rate R_{TN} = TN/N (number of correctly predicted debris flow non-occurrence – true negatives – TN over the total number of non-occurrences N) and ranges between 0 (no correct prediction) and 1 (all predictions correct):

$$bAcc = \frac{R_{TP}+R_{TN}}{2} \quad \text{(Eq.8)}$$

The sensitivity of thresholds to event occurrence was estimated using a *k*-fold fitting strategy. For each catchment, the threshold parameters α and ß were fitted on a sample of 5/6 (~83%) of the available time series in that catchment as described above. More specifically, in ID1 and ID3, the thresholds were fitted on a sub-set of 15 out of 18 available years, while in ID2 this was done using 15 out of 18 contiguous 14-day periods. This was repeated *k* times, so that each of the possible *k* combinations of 15 years (or 14-day periods in ID2) in that catchment was used for fitting. To account for threshold uncertainties arising from uncertainties in variables obtained from the hydrological model, i.e. P_R, P_L, S_U and Q, values for these variables were for each time step in each *k* fold sampled from the likelihood weighted ensemble of all retained solutions. The same strategy was used for the regional thresholds based on the combined debris flows from all three catchments. To ensure balanced samples the only difference in that case was that the sampling for the *k* folds was stratified so the samples represented 15 years (or 14-day periods) of the observed debris flows of *each* catchment in each of the *k* realizations. For both cases the results are reported in terms of the median threshold and the 5/95th uncertainty interval around it.

5 Results

5.1 Hydrological Model performance

The models robustly reproduce the overall hydrological response pattern in the three study catchments ID1c, ID2c and ID3c. In particular, the presence of snow cover and thus the dynamics of snowline elevation E_{SL} are captured with a rather high degree of accuracy with E_{SC} = 0.88 – 0.95 for calibration (Table 2) as shown in Figure 5c for the year 2021 for ID2c and in Supplementary Material Figures S1 and S2 for the other catchments. In other words, the overall best performing solutions, i.e. the lowest D_E, correctly represent the presence of snow across all elevation bands in between 88% (ID1c) and 95% (ID2c) of the timesteps. More importantly, the models' ability to mimic the presence of snow cover remains with E_{SC} = 0.91 – 0.93 as robust for the out-of-sample model evaluation and testing periods (Table 2). The models also reproduce stream flow magnitudes with $E_{NS,Q}$ between 0.77 (ID2c; Fig.5d,e) and 0.87 (ID1c) as well as the main features of the stream water level dynamics with R^2_{WL} between 0.49 (ID1c) and 0.75 (ID2c; Fig.5d,f) in a plausible, albeit due to data limitations, in a less rigorous way. In addition, the modelled mean runoff ratios over the model periods in the three study catchments are with C_R ~ 0.51 – 0.80 (Table 1) broadly consistent with observed long-term mean runoff ratios of comparable catchments in the region (e.g. Hanus et al., 2021; Ponds et al., 2025).

https://doi.org/10.5194/egusphere-2026-5589
Preprint. Discussion started: 24 September 2026

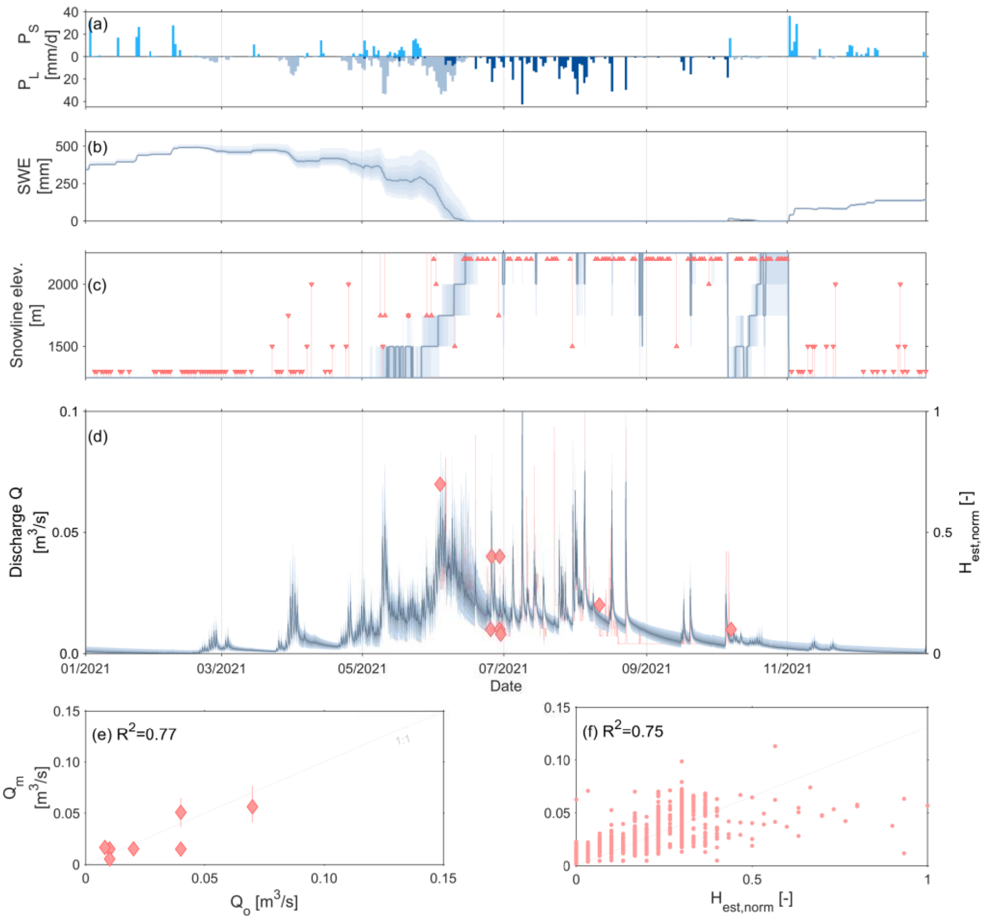

Figure 5. Modelled and observed variables for the 2021 calibration period in ID2c – Loechertroggraben catchment. (a) modelled snowfall P_S (light blue) and liquid precipitation P_L, distinguishing snow melt (light grey-blue) and rainfall (dark blue), (b) modelled snow water equivalent SWE, (c) modelled (blue) and observed (red triangles) snow line elevation E_{SL}. On days with full cloud cover no E_{SL} observation available. On days with partial cloud cover E_{SL} cannot be unambiguously determined and only its lower (upward pointing red triangles) and/or upper limits (downward pointing red triangles) are known. Only on days without cloud cover E_{SL} is unambiguously determined: when the catchment is partially snow covered the upward and downward pointing triangles coincide, when there is no snow cover the upward pointing triangles coincide with the highest elevation and when there is 100% snow cover, the downward pointing triangles coincide with the lowest elevation. (d) modelled (blue) and observed stream discharge Q (red diamond symbols) as well as normalized observed water levels $H_{est,norm}$ (red line), (e) observed vs. modelled stream discharge Q, with error bars indicating the 5/95th model uncertainty interval and (f) observed water levels $H_{est,norm}$ vs. modelled stream discharge Q. The dark blue lines in (b)-(d) indicate the median of all retained model solutions and the blue shaded areas the associated 5/95th uncertainty intervals.

https://doi.org/10.5194/egusphere-2026-5589
Preprint. Discussion started: 24 September 2026

5.2 Hydrological regimes of debris flow initiation areas

Rescaling the models calibrated for the overall catchments ID1c-ID3c to the sub-catchments ID1-ID3, allowed to describe the hydrological regimes characterizing the debris flow initiation areas and to analyse the individual modelled hydrological variables P_R, P_L, S_U and Q for their role as potential debris flow triggers. The results are shown as long-term average regime curves in Figure 6 and for a selected year (2021) in Figure 7. All other years are shown in Supplementary Material Figures S3-S19.

For both the Hopfgartnergraben (ID1) and Loechertroggraben catchments (ID2), snow accumulation typically starts towards end of October, with occasional snowfall P_S occurring until end of May (Figs.6a,b; 7a,b). In these two catchments, the seasonal snowpack over the study period reaches an annual maximum SWE around mid of March. Around that period snow melt P_M starts to reduce SWE at lower elevations while continued snow fall P_S further increases SWE at higher elevations. For the two catchments this leads to only minor net catchment-aggregated SWE reductions over all elevation zones until mid of April, when snow melt P_M finally also sets in at higher elevations. Catchment-wide snow melt that typically extends over periods of six to eight weeks then leads to a rapid decline of SWE from mid-April onwards. However, it can be observed that snow melt-out occurs around two weeks earlier, on average, in the Loechertroggraben catchment (ID2; Fig.6e, 7e) than in the Hopfgartnergraben catchment (ID1; Fig.6d, 6d), which, due to comparable SWE, entails somewhat higher snow melt rates in ID2. These seasonal dynamics of snow accumulation and melt regulate spring and early summer soil moisture dynamics S_U in similar ways in ID1 and ID2. In both cases a characteristic minimum S_U occurs around the same period as maximum SWE mid of March (Fig.6g,h), when precipitation remains stored as snow but increasing canopy water demand leads to increased soil water uptake by vegetation. Once snow melt sets in, relative soil moisture S_U sharply increases and eventually stabilizes at elevated levels of > 0.5, until most of the snow has disappeared in June (Fig.6g,h; 7g,h). This is accompanied by a gradual shift between the relative contributions of snow melt P_M and rainfall P_R to liquid water input P_L. Until mid of June, P_M is the dominant contribution to P_L, i.e. $P_M/P_L \geq 0.5$ (Fig.6a,b; 7a,b), providing persistent liquid water input over prolonged time periods. After that rainfall becomes more dominant, i.e. $P_M/P_L < 0.5$, leading to more irregular P_L input pattern due to the more intermittent nature of rainfall. Depending on the timing of summer rainfall events, high vegetation water uptake, due to higher summer temperatures, causes pronounced declines in S_U before rainstorms replenish soils again in several summer wetting-drying cycles. This results in systematic differences between spring and summer S_U dynamics, with a more pronounced fluctuation of S_U between mid of June and October as compared to the more stable (Fig.6g) or increasing S_U levels (Fig.6h) in spring during the melt period. The persistently elevated S_U levels throughout much of the snow melt period further sustain similarly persistent elevated stream flow rates Q, considerably exceeding annual average daily flow rates over several weeks in late spring and early summer (Fig.6j,k; 7j,k). The on average lower but more variable stream flow Q after the melt period reflects the more variable S_U dynamics during that period and thus the frequent drying and wetting cycles controlled by interplay of vegetation water demand and the irregular occurrence of often high intensity mid- to late summer rainstorms that typically also lead to the highest stream flow peaks in individual years.

https://doi.org/10.5194/egusphere-2026-5589
Preprint. Discussion started: 24 September 2026

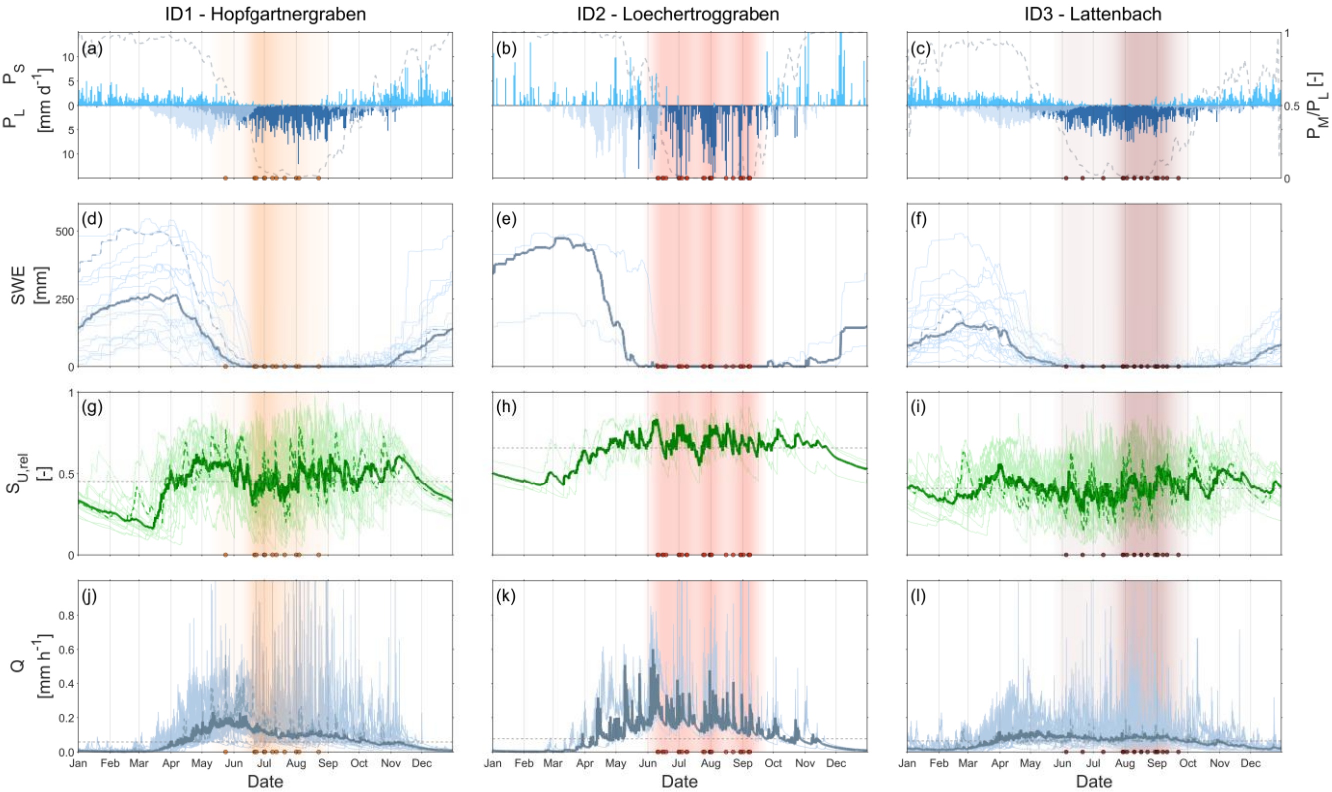

Figure 6. Hydrological regimes of the three study catchments ID1 – ID3 over the study period. (a) – (c) long-term average snowfall P_S (light blue) and liquid precipitation P_L, distinguishing snow melt (light grey-blue) and rainfall (dark blue), the dashed line indicates the fraction of snowmelt to the total liquid water input, i.e. P_M/P_L; (d) – (f) snow water equivalent SWE of the individual years of the study period 2005-2022 (thin lines), average SWE over all study years (bold lines), average SWE over the 2020-2022 period for ID1 and ID3 (dashed lines) to allow direct comparison with ID2; (g) – (h) relative soil moisture S_U of the individual years of the study period 2005-2022 (thin lines), average S_U over all study years (bold lines), average S_U over the 2020-2022 period for ID1 and ID3 (dashed green lines) to allow direct comparison with ID2 and the long-term annual average S_U (dashed grey lines); (j) – (l) stream flow Q of the individual years of the study period 2005-2022 (thin lines), average Q over all study years (bold lines), average Q over the 2020-2022 period for ID1 and ID3 (dashed green lines) to allow direct comparison with ID2 and the long-term annual average Q (dashed grey lines). The circle symbols indicate the observed debris flows in ID1 (orange), ID2 (red) and ID3 (dark red), respectively, throughout the study periods. The associated orange, red and dark red shaded areas indicate kernel density distribution estimates of debris flow occurrence probability for visualization purposes.

https://doi.org/10.5194/egusphere-2026-5589
Preprint. Discussion started: 24 September 2026

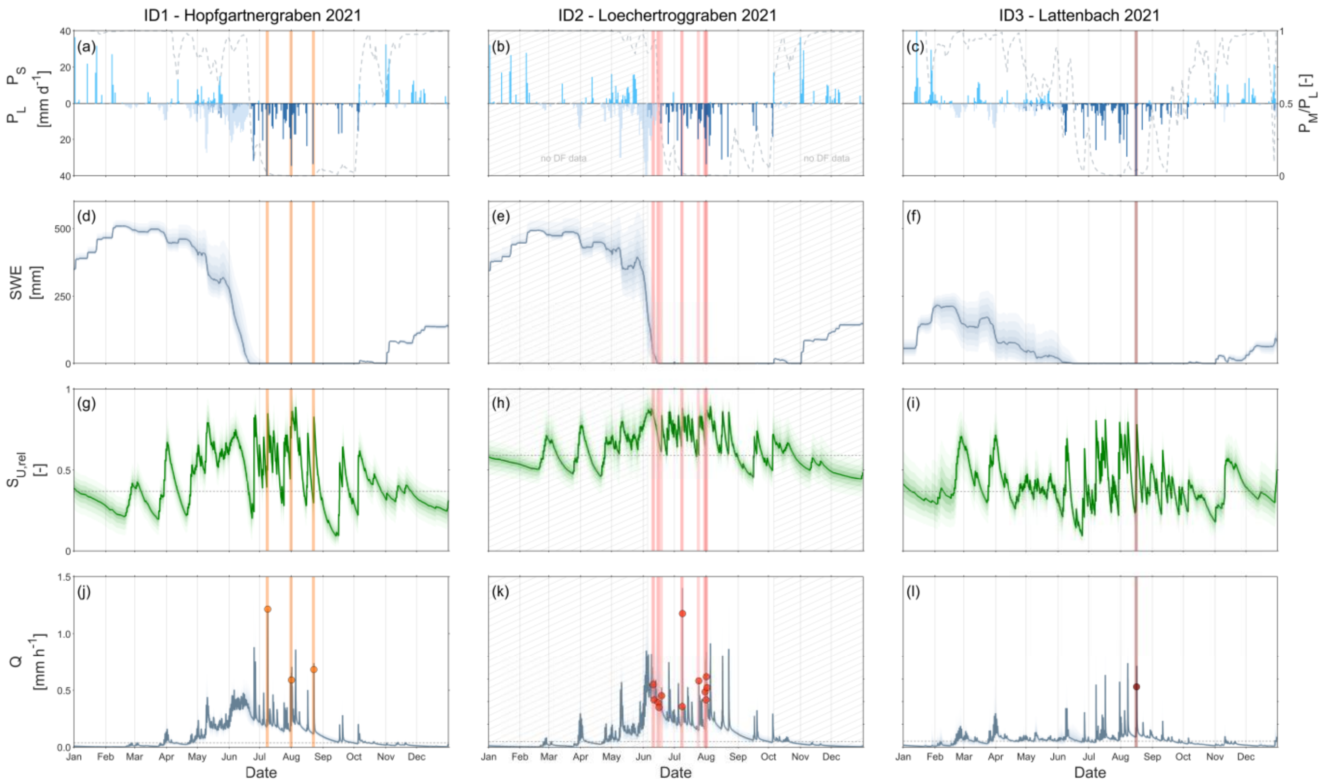

Figure 7. Hydrological variables of the three study catchments ID1 – ID3 for the year 2021. (a) – (c) median modelled snowfall P_S (light blue) and liquid precipitation P_L, distinguishing snow melt (light grey-blue) and rainfall (dark blue), the dashed line indicates the fraction of snowmelt to the total liquid water input, i.e. P_M/P_L; (d) – (f) median modelled snow water equivalent SWE (solid blue line) and the 5/95th uncertainty interval (blue shaded area); (g) – (h) median modelled relative soil moisture S_U (solid green line), the 5/95th uncertainty interval (green shaded area) and the 2021 average S_U (dashed grey line); (j) – (l) median modelled stream flow Q (solid blue line), the 5/95th uncertainty interval (blue shaded area) and the 2021 average Q (dashed grey lines). The orange (ID1), red (ID2) and dark red bars (ID3) indicate the date of observed debris flows and the circle symbols indicate the median modelled channel stream flow Q associated with each debris flow.

In the Lattenbach catchment ID3, the hydrological regime exhibits somewhat different characteristics. Drier and receiving somewhat less winter precipitation (Tab. 1), annual average snowfall P_S in ID3 is ~400 mm yr^{-1} while in the other catchments annual average P_S is ~25% higher, reaching ~500 mm yr^{-1}. The correspondingly lower average annual maximum SWE (Fig.6f) and associated average annual P_M have cascading effects on S_U. This is further exacerbated by markedly lower snow melt intensities (Fig.6c,f; 7c,f) that result from a combination of lower SWE and longer melt periods. The latter are largely a consequence of the wider elevation range in ID3, with ~30% of the catchment being located at lower elevations than the lowest elevations of ID1 and ID2, respectively (Fig.1, Table 1). The associated higher temperatures at lower elevations cause earlier onset of P_M, typically starting from mid of February (Fig.6c, 7c). As a consequence, P_R becomes the dominant water input, i.e. $P_M/P_L < 0.5$, around mid of May and thus one month earlier than in ID1 and ID2. Together, the above factors lead to markedly different seasonal S_U dynamics in ID3 than in the other two catchments. While snow melt P_M also replenishes soils in ID3 until end of March (Fig.6i), the S_U increase is less pronounced as compared to ID1 and ID2. As a specific feature of ID3 it is observed that P_M rates decline from end of March onwards (Fig.6c, 7c), at the same time that vegetation water demand starts to increase. In contrast to ID1 and ID2, this leads to declining S_U throughout the remaining snow melt period and until around mid of June, when the lowest annual S_U levels are reached (Fig.6i, 7i) and when the magnitudes and frequencies of summer rainstorms start to increase (Fig.6c, 7c). The lower overall S_U levels, the declining spring S_U levels as well as the weaker contrast between winter and summer S_U levels in ID3 are responsible for the absence of the systematic and prolonged summer high flows (Fig.6l, 7l), which are characteristic for ID1 and ID2. Although the timing and magnitudes of annual maximum flows are similar to those of ID1 and ID2, the absence of the pronounced and prolonged summer high flow period in ID3 further illustrates the dominance of more erratic rainfall P_R input instead of more persistent snow melt P_M as critical control on the hydrological regime in ID3.

5.3 Emergent debris flow regimes

Analysis of debris flow events in the Hopfgartnergraben catchment (ID1) during the 18-year study period revealed that all the 12 observed debris flows occurred in the 3-month period between end of May and end of August (Figure 8a). Overall, the frequency of debris flow occurrences is highest between mid-June and mid-July with a median date of occurrence being July 7 (Figure 8d). In contrast, the wettest conditions in a year, here defined as timesteps with $P_{L,i}$ and Q both exceeding lowest $P_{L,i}$ and Q at the moment of observed debris flows in that catchment, have throughout the study years been observed to occur between end of June and beginning of September, with a median date of August 10 (Figure 8d). On average, debris flows therefore occur more than one month (Δt = 33 d) before the wettest conditions in a year (Figure 8g). Thus, although ~60% of debris flows occurred at discharge magnitudes exceeding the 99th quantile (Figure 8j), and therefore under very wet conditions, the vast majority was triggered early in the season, in spite of similar or even more extreme wetness conditions regularly occurring much later in the year but rarely triggering debris flows after mid-August. This suggests that from August onwards, sediment supply is exhausted by previous debris flows and not sufficiently and not fast enough resupplied to the channel at that time of the year. Rather, the persistent wet conditions in spring and early summer (Figure 6g,j), with both S_U and Q above their annual averages for typically several weeks, although not extreme, are likely to be responsible for a gradual sediment supply throughout that period by transferring debris from the hillslope into the channel system. The sediment that is then accumulated close to or in the channel is remobilized as debris flows under early summer wet, albeit not necessarily extreme, conditions. In this case the lack of sufficient sediment resupply from mid-summer onwards then causes a rather weak coupling between wetness extremes that to a large part occur later in summer and the occurrence of debris flows (Figure 8g).

In the Loechertroggraben catchment (ID2), debris flows have been observed between beginning of June end mid-September across the study years (Figure 8b). Note that in ID2 it is possible that debris flows, that may have occurred earlier in the year, were missed due to logistical constraints that generally prevent access to the catchment and thus observations before end of May. In contrast to ID1, the occurrence of debris flows spreads rather homogeneously over the summer months, with a median date of occurrence on July 25 (Figure 8e) and thus around three weeks later than in ID1. The wettest conditions dominantly occur, on average, in early summer, with a median date of July 2 (Figure 8e) and thus much earlier than in ID1. In addition, and in contrast to ID1, these conditions temporally coincide with the persistent early summer wet period (Figure 6h,k). Together, these factors lead to the situation that in ID2 the wettest extremes in a year typically precede debris flows by a few days (Δt = - 9d; Figure 8h). In spite of the somewhat stronger temporal coupling between the respective timing of extreme wetness and debris flow occurrences than in ID1, it can be observed that in ID2, only ~30% of the debris flows occur at discharge magnitudes above the 99th percentile (Figure 8k), and more than 50% occur at discharge magnitudes well below the 95th percentile (Figure 8k). This at first glance counterintuitive result implies that a considerable fraction of debris flows occurs under wetness conditions that are not necessarily extreme. We hypothesize that extremes that occur several days before debris flows may cause a rapid sediment resupply into the main channel through an upstream dense network of gullies within the unvegetated source area throughout the season. Once sufficient sediment is then available in a channel reach with sufficient contributing area and an equilibrium between sediment and transport capacity, i.e. discharge, is reached, less extreme conditions can then trigger debris flows in the channel.

In the Lattenbach catchment (ID3), debris flow occurrences largely concentrate in late summer with a median date of occurrence on August 15, with only occasional debris flows as early as end of June (Figure 8c,f), and thus much later than in the other two study catchments. Here, the occurrence of debris flows temporally largely overlaps with the occurrence of annual extreme wetness conditions over the years, which exhibit a median date of occurrence on August 19 (Figure 8f). On average, individual debris flows have occurred with a delay of merely Δt = -1d after such very wet conditions (Figure 8h). In other words, and in contrast to ID1 and ID2, the occurrence of debris flows is temporally strongly coupled to the occurrence of annual wetness extremes in ID3. The strength of the coupling is further illustrated by the fact that >65% of debris flows have occurred at discharge magnitudes exceeding the 99th percentile (Figure 8l). Until July, moderate wetness conditions with declining S_U generate only occasional channel flow peaks. This is likely to restrict both, in-stream transport capacity for debris flow initiation and sediment resupply from the embankment (i.e. toe of deep-seated landslides). At the same time, snowmelt

https://doi.org/10.5194/egusphere-2026-5589
Preprint. Discussion started: 24 September 2026

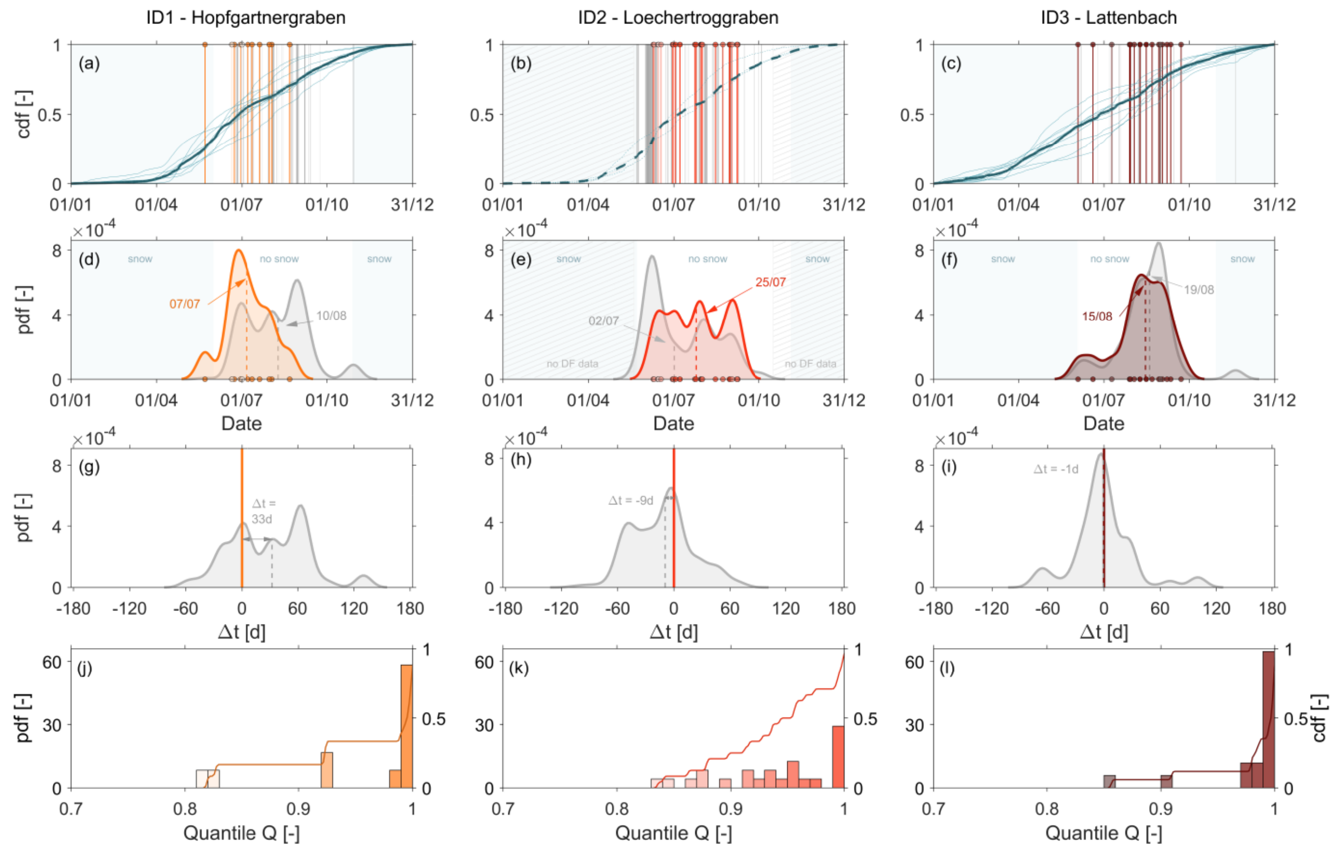

Figure 8. Debris flow regimes in study catchments ID1 – ID3, as characterized by seasonal timing of debris flow occurrence and associated wetness conditions. (a) – (c) timing of observed debris flows (orange/red bars), timing of wettest annual conditions (grey bars), i.e. timesteps when both $P_{L,i}$ and Q exceeded the minimum debris flow triggering $P_{L,i}$ and Q in each catchment, period with snow cover (light blue shaded areas) and cumulative P_L for the individual study years (thin blue lines) as well as long-term average annual cumulative P_L (bold blue line) over the study period. The grey hatched area in (b) indicates periods with no active monitoring and thus with no debris flow data available, as also indicated by the dashed blue lines; (d) – (f) frequency distributions of debris flow occurrences (orange/red shaded areas) together with the median dates of occurrence (orange/red dashed lines) as well as frequency distributions of the timing of wettest annual conditions (grey shaded areas) together with the median data of occurrence (grey dashed line), circle symbols indicate the dates of the individual debris flows; (g) – (i) frequency distributions of time lags of wettest annual conditions (grey shaded areas) relative to the timing of individual debris flows (orange/red bars) in their respective years of occurrence, grey dashed lines indicate the median time lag; (j) – (l) frequency distributions of debris flow triggering channel discharge Q quantiles (orange/red bars) and the cumulative distribution of debris flow triggering Q quantiles (orange/red lines).

https://doi.org/10.5194/egusphere-2026-5589
Preprint. Discussion started: 24 September 2026

sustains elevated baseflow early in the year, with a maximum in May (Fig.6l), which promotes the continuous export of finer fractions of in-channel sediment from the catchment by fluvial activity, thereby limiting the sediment availability for debris flow initiation. In other words, the divergence of the snowmelt period and the period of extreme, mostly convective, rainfall events, shifts the probability of debris flow initiation to late-summer. S_U and thus wetness levels increase above annual average again only from August onwards (Figure 6i) when increasing frequency and magnitude of summer rainstorms offsets vegetation water demand and leads to increased frequency and magnitudes of discharge peaks (Figure 6l). The increasing frequency of debris flows around that same, well-defined period, is consistent with the interpretation that sediment resupply earlier in the year is insufficient for the available in-stream transport capacity to cause debris flows. Only the higher frequency and magnitude of late summer rainstorms provide both sufficient sediment as well as discharge and thus in-stream transport capacity to cause debris flows.

5.4 Debris flow initiation thresholds

5.4.1 Regional vs. local thresholds

The six individual types of regional thresholds in the general form of $y = \alpha x^{\beta}$, obtained from the combined set of debris flows from all three study catchments (Supplementary Material Fig.S20), differ systematically but to varying degrees from the local thresholds individually obtained for the three study catchments as shown in Figures 9-11. As the regionally derived scale parameters α are consistently lower than the local ones in all three catchments (Figure 12), the regional thresholds plot mostly below the local thresholds (Figures 9-11). With $\Delta\alpha < 0.5$ between regional and local thresholds, the differences remain limited in ID1 and become most apparent for the Q-$P_{L,i}$ threshold (Figure 9e, 12a). For ID2 and ID3, the differences are generally more pronounced reaching a maximum of $\Delta\alpha \sim 4.2$ for the $P_{R,d}$-$P_{R,i}$ threshold in ID2 (Figure 10b, 12b) and $\Delta\alpha \sim 0.9$ for the P_d-P_i threshold in ID3 (Figure 11a, 12c). Overall, in ID1 the differences between regional and local α are larger for thresholds that include hydrological information, i.e. S_U-$P_{L,i}$ and Q-$P_{L,i}$, while in ID2 and ID3 thresholds based exclusively on precipitation information, i.e. P_d-P_i, $P_{R,d}$-$P_{L,i}$ and $P_{L,d}$-$P_{L,i}$, exhibit the largest Δα (Figure 12). Although the absolute difference Δß between the scale parameters ß of regional and local thresholds remains limited in ID1, local ß values are lower for all threshold types (Figure 12a), resulting in systematically steeper local than regional thresholds in ID1 (Figure 9). In contrast, for ID2 and ID3, the absolute differences Δß between regional and local thresholds are not only markedly more pronounced for all threshold types, but local ß is also higher than regional ß for all threshold types except Q-S_U (Figure 12b, c), leading to flatter local threshold slopes (Figure 10, 11). The fact that the shape parameter drops to very low values that can surpass ß <-100 for the Q-$P_{L,i}$ (ID2) and Q-S_U thresholds (ID1-ID3) as shown in Figure 12, implies that these thresholds converge towards vertical slopes, effectively collapsing the 2-dimensional, bivariate thresholds to 1-dimensional and thus univariate thresholds, here de facto defined by Q as only variable (Figure 9-11), supporting the hypothesis of a critical runoff conditions for debris flow initiation (Takahashi, 1978).

https://doi.org/10.5194/egusphere-2026-5589
Preprint. Discussion started: 24 September 2026

The above-described systematic differences between regional and local thresholds lead to associated differences in the ability of regional and local thresholds to correctly detect debris flows. The regional thresholds can predict debris flow occurrence at the regional scale, i.e. across all study catchments, moderately well with bAcc = 0.83 – 0.92 and AUC = 0.80 – 0.95, depending on the threshold type (Supplementary Material Fig.S20). When using the regional thresholds to predict debris flows locally in the individual study catchments, a more nuanced picture emerges. The regional thresholds locally detect debris flows moderately well in ID1 with bAcc = 0.79 – 0.96 (Figure 9, 13g) and similar values for AUC (Figure 9, 13d) and even slightly better in ID3, with bAcc = 0.86 – 0.97 (Figure 11, 13f). In contrast, the ability of all six regional thresholds to locally detect debris flows in ID2 is substantially lower, with bAcc = 0.61 – 0.70 (Figure 10, 13h) and AUC = 0.60 – 0.81 (Figure 10, 13e). This suggests that none of the six regional thresholds captures the processes to meaningfully describe the debris flow regime in ID2.

Local thresholds across all six types and all three study catchments consistently outperform the regional thresholds (Figure 13). More specifically, in ID1, the local thresholds locally detect debris flows with bAcc = 0.81 – 0.98 (Figure 9, 13g), which is an increase of ΔbAcc ~ 0.03, on average, compared to the regional thresholds. Similarly, in ID3, bAcc was found to increase by ~0.02, on average, to bAcc = 0.86 – 0.98 (Figure 12, 13i). In both cases, the overall level of improvement in terms of bAcc thus remains similarly modest for all threshold types. In contrast, in terms of AUC, it can be observed that the two local thresholds that combine precipitation information with hydrological information, i.e. S_U-$P_{L,i}$ and Q-$P_{L,i}$, lead to considerable improvements as compared to the regional thresholds in both, ID1 (Figure 13d) and ID3 (Figure 13f), with ΔAUC as high as 0.12. A different picture emerges for ID2, where local thresholds lead to clear increases of bAcc, by ΔbAcc ~ 0.08, on average, to bAcc = 0.70 – 0.76 (Figure 13h) across all six threshold types. In addition, and comparable to ID1 and ID3, the two local, hydrology-informed thresholds, S_U-$P_{L,i}$ and Q-$P_{L,i}$, also show the strongest AUC improvements with ΔAUC ≥ 0.05 (Figure 13e).

https://doi.org/10.5194/egusphere-2026-5589
Preprint. Discussion started: 24 September 2026

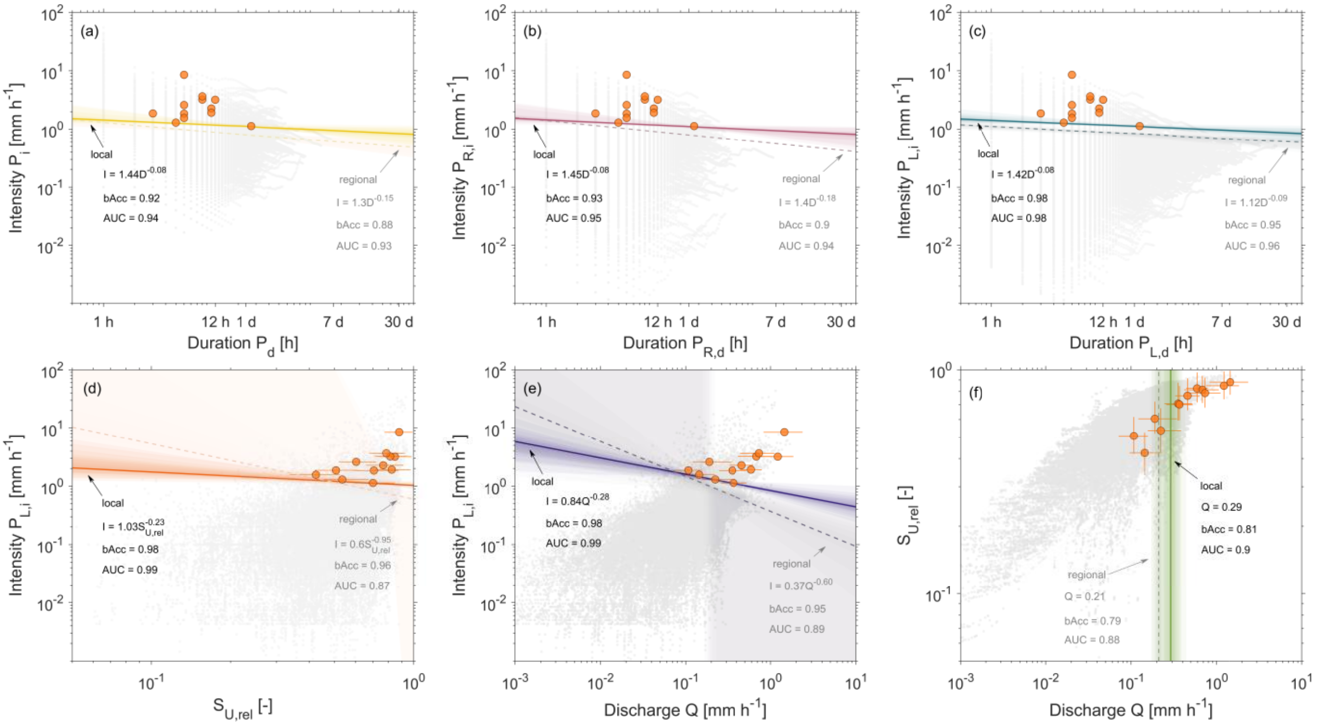

Figure 9. The six bivariate regional and local debris flow thresholds for the Hopfgartnergraben catchment (ID1). (a) precipitation duration and intensity threshold P_d-P_i, (b) rainfall duration and intensity threshold $P_{R,d}$-$P_{R,i}$, (c) liquid precipitation duration and intensity threshold $P_{L,d}$-$P_{L,i}$, (d) soil moisture and liquid precipitation intensity threshold S_U-$P_{L,i}$, (e) discharge and liquid precipitation threshold Q-$P_{L,i}$ and (f) discharge and soil moisture threshold Q-S_U. The thin dashed lines indicate the regional thresholds and the light shaded areas the associated 5^{th}-95^{th} uncertainty intervals. The bold lines show the local thresholds and the shaded areas the 5^{th}-95^{th} uncertainty intervals. The orange circles indicate observed debris flow event, representing true positives TP when plotting above and false negatives FN when plotting below the thresholds. The light grey dots indicate no-debris flow events, representing false positives FP when plotting above and true negatives TN when plotting below the thresholds. The horizontal and vertical orange error bars indicate the 5-95^{th} uncertainty of the respective modelled variables. Note, error bars of P_R and P_L not shown as the uncertainties were minor. Thresholds with $ß \leq -100$ converge towards vertical thresholds and are thus here for brevity labelled as univariate thresholds in the form of x = const.

https://doi.org/10.5194/egusphere-2026-5589
Preprint. Discussion started: 24 September 2026

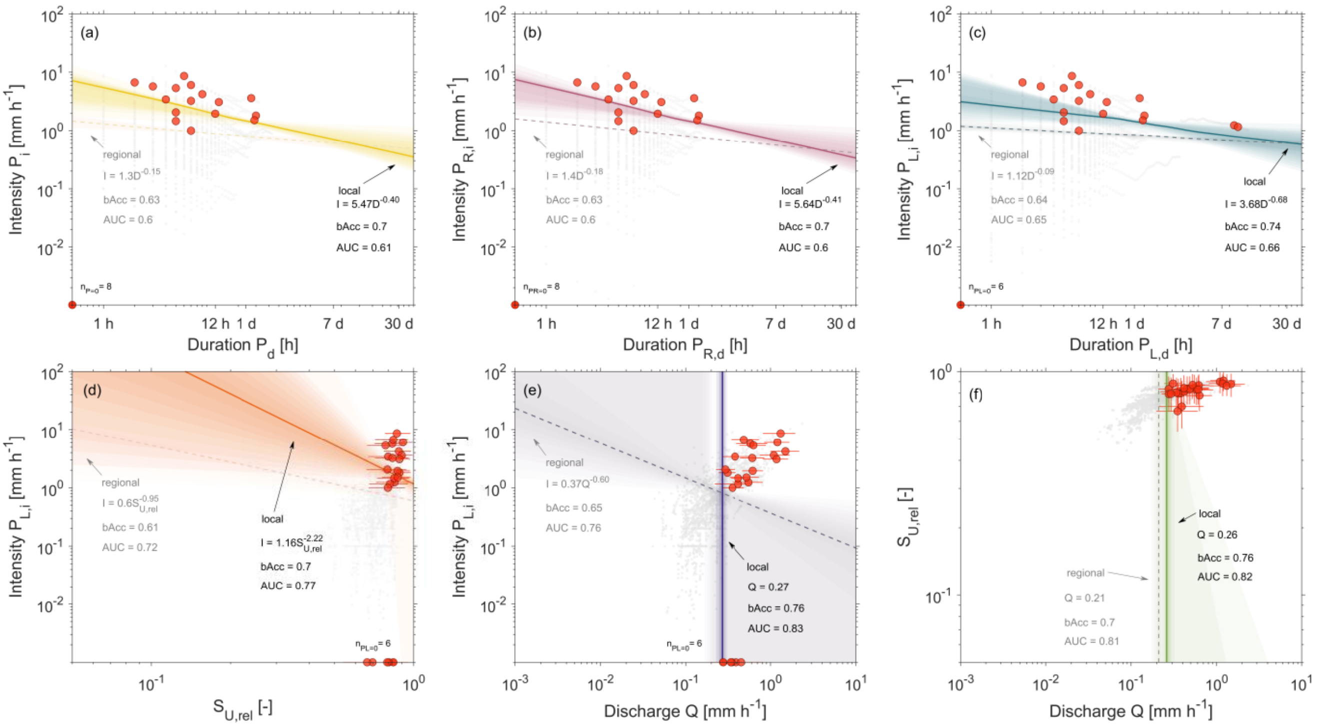

Figure 10. The six bivariate regional and local debris flow thresholds for the Loechertroggraben catchment (ID2). (a) precipitation duration and intensity threshold P_d-P_i, (b) rainfall duration and intensity threshold $P_{R,d}$-$P_{R,i}$, (c) liquid precipitation duration and intensity threshold $P_{L,d}$-$P_{L,i}$, (d) soil moisture and liquid precipitation intensity threshold S_U-$P_{L,i}$, (e) discharge and liquid precipitation threshold Q-$P_{L,i}$ and (f) discharge and soil moisture threshold Q-S_U. The thin dashed lines indicate the regional thresholds and the light shaded areas the associated 5th-95th uncertainty intervals. The bold lines show the local thresholds and the shaded areas the 5th-95th uncertainty intervals. The red circles indicate observed debris flow event, representing true positives TP when plotting above and false negatives FN when plotting below the thresholds. The light grey dots indicate no-debris flow events, representing false positives FP when plotting above and true negatives TN when plotting below the thresholds. Note that the red circles on the x-axes are an indication of debris flows that occurred in the absence of precipitation events, i.e. with duration and intensity equal to zero, here exclusively shown for illustrative purposes. The horizontal and vertical red error bars indicate the 5-95th uncertainty of the respective modelled variables. Note, error bars of P_R and P_L not shown as the uncertainties were minor. Thresholds with $ß \leq -100$ converge towards vertical thresholds and are thus here for brevity labelled as univariate thresholds in the form of x = const.

https://doi.org/10.5194/egusphere-2026-5589
Preprint. Discussion started: 24 September 2026

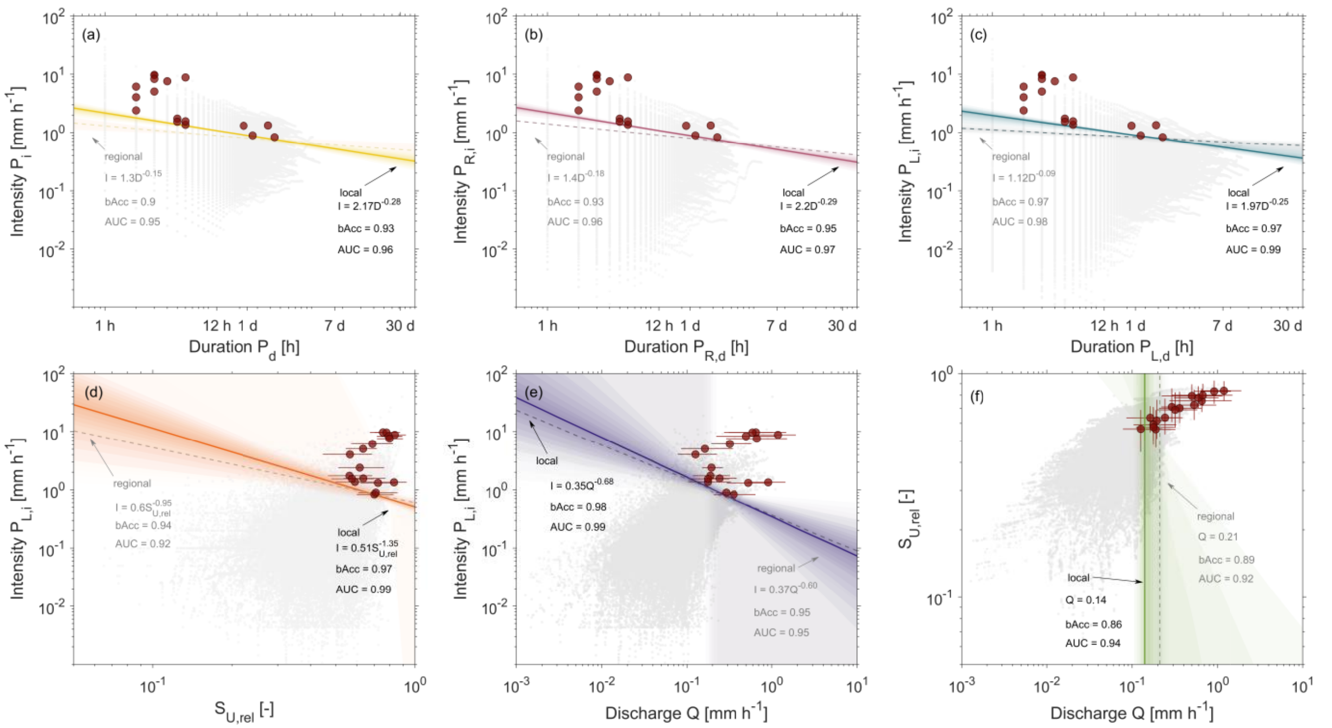

Figure 11. The six bivariate regional and local debris flow thresholds for the Lattenbach catchment (ID3). (a) precipitation duration and intensity threshold P_d-P_i, (b) rainfall duration and intensity threshold $P_{R,d}$-$P_{R,i}$, (c) liquid precipitation duration and intensity threshold $P_{L,d}$-$P_{L,i}$, (d) soil moisture and liquid precipitation intensity threshold S_U-$P_{L,i}$, (e) discharge and liquid precipitation threshold Q-$P_{L,i}$ and (f) discharge and soil moisture threshold Q-S_U. The thin dashed lines indicate the regional thresholds and the light shaded areas the associated 5^{th}-95^{th} uncertainty intervals. The bold lines show the local thresholds and the shaded areas the 5^{th}-95^{th} uncertainty intervals. The dark red circles indicate observed debris flow event, representing true positives TP when plotting above and false negatives FN when plotting below the thresholds. The light grey dots indicate no-debris flow events, representing false positives FP when plotting above and true negatives TN when plotting below the thresholds. The horizontal and vertical dark red error bars indicate the 5-95^{th} uncertainty of the respective modelled variables. Note, error bars of P_R and P_L not shown as the uncertainties were minor. Thresholds with $ß \leq -100$ converge towards vertical thresholds and are thus here for brevity labelled as univariate thresholds in the form of x = const.

https://doi.org/10.5194/egusphere-2026-5589
Preprint. Discussion started: 24 September 2026

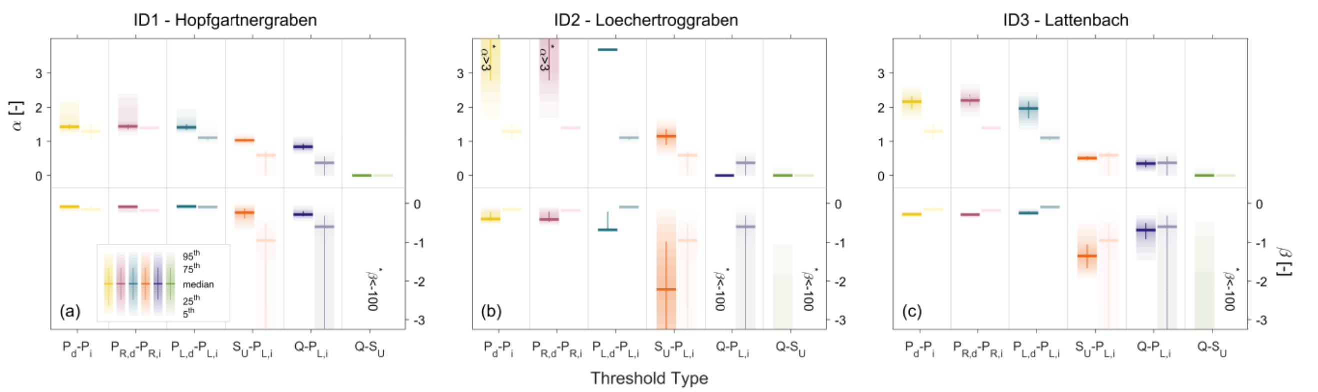

Figure 12. Regional and local scale (α) and shape parameters (ß) for all six threshold types in (a) Hopfgartnergraben catchment (ID1), (b) Loechertroggraben catchment (ID2) and (c) Lattenbach catchment (ID3). The left boxplots show local parameters and the right boxplot the regional parameters for each threshold type. The bold lines indicate the median of all retained solutions and the shaded areas the 5th-95th uncertainty interval. Note, that for values $ß \leq -100$, threshold converge towards vertical and thus univariate thresholds.

5.4.2 Performance of different threshold types

As shown in Figure 13, the overall performance pattern1 of both, local and regional thresholds for the six different threshold types is consistent across the three study catchments. For brevity only the performance of local thresholds is described in the following. Not unexpectedly, the precipitation thresholds P_d-P_i (Figure 9a-11a, 13) exhibit with AUC = 0.61 – 0.96 (Figure 13d-f) and bAcc = 0.70 – 0.93 (Figure 13g-i) lower skill to detect debris flows than most of the other thresholds in the study catchments. In ID1 and ID2, this is mostly a consequence of elevated false positive rates of up to $R_{FP} \sim 0.18$ (Figure 13a, c). In other words, up to ~18% of all time steps with no observed debris flows are wrongly identified as debris flow events (“false alarms”). In contrast, the poor performance in ID2, with AUC = 0.61, which is only marginally stronger than random guessing (AUC = 0.50), can be to large part be attributed to this threshold’s failure to detect 8 of 24 observed debris flows in ID2, i.e. 33%. This elevated number of false negatives, or in other words, missed debris flows, is mostly a result of the absence of precipitation when these debris flows occurred (Figure 10a). Exclusively considering rainfall, the $P_{R,d}$-$P_{R,i}$ thresholds do only result in very minor improvements in all study catchments (Figure 9b-11b, 13). Instead, significantly higher threshold performances ($p < 0.05$) were achieved throughout the three catchments when using liquid water input P_L and thus explicitly accounting for rainfall plus snow melt as $P_L = P_R + P_M$. More specifically, in ID1 and ID3 the $P_{L,d}$-$P_{L,i}$ thresholds lead to very robust thresholds with AUC = 0.96 – 0.99 (Figure 13d,f) and bAcc = 0.95 – 0.97 (Figure 13g,i). This is largely a consequence of the reduction of false positive rates by > 0.10 to $R_{FP} \sim 0.05$ (Figure 13a,c) and thus ~66% less false alarms with $P_{L,d}$-$P_{L,i}$ thresholds than with the P_d-P_i and $P_{R,d}$-$P_{R,i}$ thresholds. Although the overall skill with AUC = 0.66 (Figure 10c, 13e) and bAcc = 0.74 (Figure 10c, 13h) remains below the performances in ID1 and ID3, the $P_{L,d}$-$P_{L,i}$ threshold provides nevertheless

https://doi.org/10.5194/egusphere-2026-5589
Preprint. Discussion started: 24 September 2026

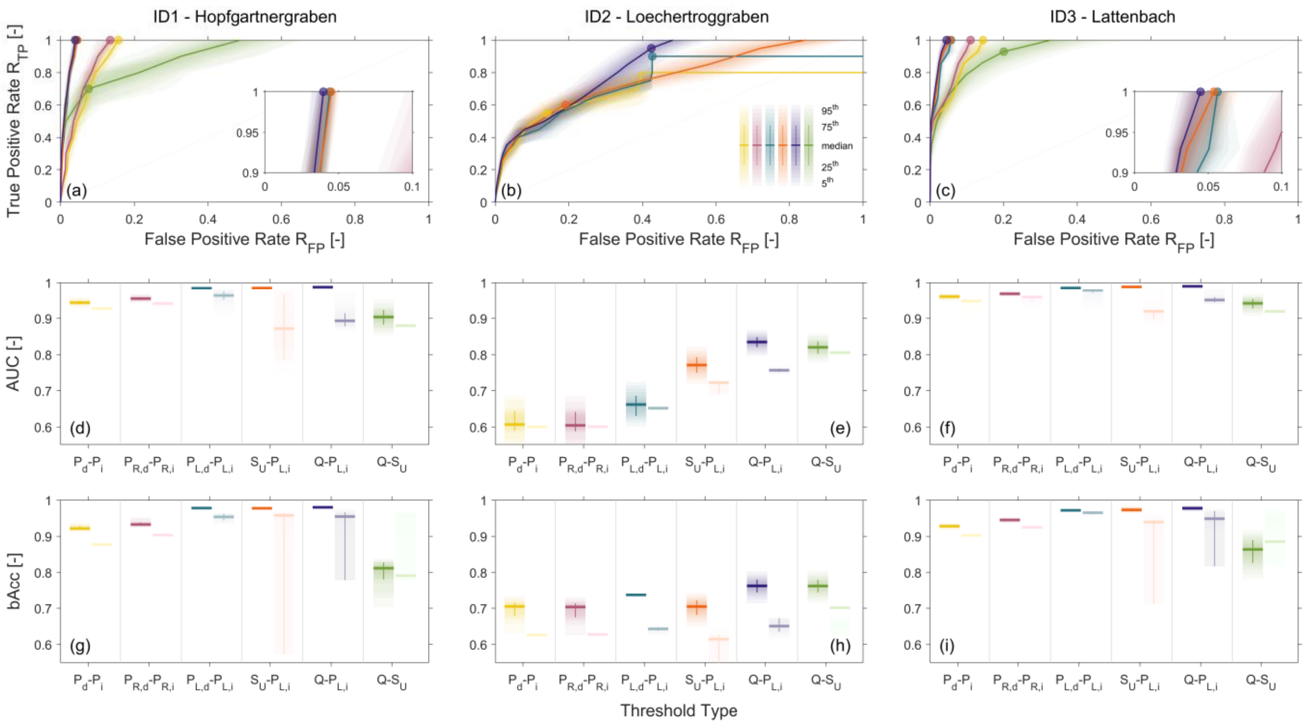

Figure 13. Performance metrics of all six threshold types across the study catchments. (a)-(c) Receiver operating characteristic curves of the six local threshold types. The insets in (a) and (c) show are zoomed in. In (b) the $P_{R,d}$-$P_{R,i}$ and Q-S_U thresholds were omitted for clarity, as they largely overlapped with the other thresholds. (d)-(f) Area-Under-Curve (AUC) metric and (g)-(i) Balanced Accuracy (bAcc) for all threshold types. The bold lines indicate the median of all retained solutions and the shaded areas the 5th-95th uncertainty interval. The left boxplots of each colour show the local and the right boxplots the regional thresholds.

considerable improvements in ID2 compared to the P_d-P_i and $P_{R,d}$-$P_{R,i}$ thresholds. The improvements in ID2 are a direct result of the identification of snow melt events that were temporally associated with two observed debris flows. Accounting for P_M then lead to $P_L = P_R + P_M > 0$ mm hr^{-1} for these two debris flows for which no precipitation ($P = 0$ mm hr^{-1}) or rainfall ($P_R = 0$ mm hr^{-1}) where observed. This reduced the number debris flows with zero (and thus undefined at the logarithmic scale of the thresholds) observed water input and eventually increased R_{TP} (Figure 13b) and thus the correctly identified debris flows.

With the inclusion of hydrological information and in particular discharge Q as variable in the thresholds, further improvements for the detection of debris flows were achieved. The most pronounced effects were found in ID2, where AUC substantially increased to 0.83 (Figure 10e, 13e) and bAcc to 0.76 (Figure 10e, 13h) for the Q-$P_{L,i}$ threshold, as a result of both, reduced false positive rates R_{FP} as well as increased true positive rates R_{TP}. Note, that assuming for $ß \leq -100$ the thresholds become vertical and thus univariate in the form Q = const. also allowed to account for the debris flows with no water input (i.e. $P_L = 0$ mm hr^{-1}), which otherwise would have remained undefined at the logarithmic scale of the thresholds. Similarly strong improvements were found in ID2 when also including soil moisture information with AUC = 0.77 for the S_U-$P_{L,i}$ and 0.82 for

https://doi.org/10.5194/egusphere-2026-5589
Preprint. Discussion started: 24 September 2026

the S_U-Q thresholds, respectively (Figure 10e, 13e). In ID1 and ID3 the threshold performance also further increased for the Q-$P_{L,i}$ and S_U-$P_{L,i}$ thresholds (Figure 9d-e, 11d-e) to AUC ≥ 0.99 (Figure 13d,f) and bAcc = 0.97 – 0.98 (Figure 13g,i), respectively, by a further reduction of false alarms and thus false positive rates to R_{FP} ~ 0.04 (Figure 13a,c). In contrast to ID2, the Q-S_U thresholds are characterized by significantly lower performances than all other thresholds in ID1 and ID3, with AUC ≤ 0.94 and bAcc ≤ 0.86.

6 Discussion

6.1 Interpretation of debris flow regimes

The pronounced differences in seasonal timing of debris flows across the study catchments (Figure 8) reflect the previously well described importance of local climatic conditions and large-scale weather pattern as first order control on the occurrence of debris flows (e.g. Prenner et al., 2018; Nikolopoulos et al., 2015). The results suggest a major role of winter precipitation accumulating in snowpacks and released as snow melt in early summer as also similarly reported by Mostbauer et al. (2018) and Prenner et al. (2019) for the wider region. These two earlier studies directly attribute many early summer debris flows to be directly triggered by high-intensity snowmelt events. However, individual snowmelt and even rain-on-snow events rarely temporally coincide with the occurrence of debris flows in our study channels as can be seen in Figures 6 and 7. This suggests that snowmelt itself is unlikely to be a *direct* trigger of debris flows in the study regions. Instead, the gradual melting of the snowpack over periods of around two months provides a steady supply of water to the subsurface. As this happens during a time of the year when atmospheric water demand for evaporation, i.e. E_P, is not yet at its maximum, this is in ID1 and ID2 sufficient to avoid drying of soils and to sustain elevated soil moisture as well as groundwater levels and thus a high level of hydrological connectivity (Figures 6,7). As a consequence, little additional water can be stored in the subsurface, resulting in fast and pronounced stream discharge peaks and thus high in-stream transport capacity in response to rainfall, which is in ID1 and ID2 further exacerbated by the steep mean channel slopes in the source areas of 33.8° and 37.6°, respectively (Tab.1). In addition, the high soil moisture levels cause elevated, i.e. not very negative pore pressure over prolonged periods. It can therefore here be plausibly hypothesized that the latter, together with the steepness of the terrain, facilitates the supply and accumulation of loose sediment to the channel through hillside erosion, small landslides, bank collapse or other mechanisms. The combination of both, sufficient sediment deposited close to the angle of repose, and transport capacity, i.e. sufficient discharge Q at steep slopes to remobilize that sediment, available in the channel as result of a melting snowpack, then creates conditions that favour the triggering debris flows.

Consistent with the above reasoning, the much lower levels of winter precipitation and thus smaller snowpacks in ID3, which is with 18.3° mean channel slope in the source area also much less steep than ID1 and ID2, lead to markedly different seasonal debris flow dynamics. Less melt water input due to smaller snowpacks and earlier melt leads to comparatively low spring soil moisture levels and further drying of soils throughout early summer, before intensity and frequency of summer rainstorms

https://doi.org/10.5194/egusphere-2026-5589
Preprint. Discussion started: 24 September 2026

increase, eventually leading to late summer increases of soil moisture levels in ID3. The snowmelt-sustained, relatively high baseflow throughout spring, with only occasional peaks, has the potential to wash-out sediment from the moderately steep channel without reaching sufficient transport capacity to initiate debris flows early in the year. These results suggest that pronounced soil moisture deficits and thus also low pore pressures, that develop in early summer due to a lack of further snowmelt, in combination with the only occasional and irregular occurrence of high intensity rainstorms before late summer severely limit both, sediment supply to and transport capacity, i.e. Q, in the moderately steep channel of ID3 and lead to much later occurrence of debris flows. Overall, these results suggest that snowpack and snowmelt are critical controls for the timing of debris flows in the study channels, albeit less as *direct* debris flow trigger but rather as a dominant factor that regulates seasonal timing of sediment supply, sediment depletion, and in-stream transport capacity in the channel. As such, snow and the associated soil moisture dynamics are here interpreted as major factors that shape the climatic predisposition to debris flows in the study channels.

The differences in timing of debris flow occurrence relative to the timing of the wettest annual conditions across the study channels provide further mechanistic insights that have so far remained under-explored in literature. Extreme rainfall events or discharge peaks at different times in the year will have different effects on debris flow occurrence in the individual channels. In other words, the same extreme discharge peak of e.g. $Q = 0.5$ mm h^{-1}, may trigger a debris flow in June but not in September in some channels and vice versa in other, nearby channels. In ID1, debris flows occur, on average, within a rather short period of time preceding the wettest annual conditions (Figure 8). Sufficient sediment is thus available in or close to the rather steep channel (~34°), facilitating the formation of debris flows early in the year under wet, but not necessarily extreme conditions. In contrast, more extreme wetness conditions later in the year rarely trigger debris flows. This observation suggests that sediment is soon exhausted and cannot be sufficiently resupplied to the channel before the next winter/spring periods (observed mean debris flow frequency of ~0.67 yr^{-1}). As the late summer wetness conditions, the steep terrain and thus the in-stream transport capacity exceed the levels necessary to trigger debris flows, the debris flow regime is limited by insufficient sediment in late summer. The effective de-coupling of extreme wetness conditions and debris flow occurrences are therefore a strong indicator for a sediment- and thus supply-limited debris flow regime sensu Bovis & Jakob (1999) and Qie et al. (2024), supporting our initial geomorphological assessment outlined in Sec.2. ID 2, the steepest (~38° in the source area) and most active (8 events yr^{-1}) of the studied channels, is characterized by a slightly stronger coupling. Although debris flows do, on average, more strongly coincide with wet conditions, their occurrence is much more evenly distributed over a longer period, stretching from early to late summer (Figure 8). This suggests a more dynamic balance between sediment availability and transport capacity. The several cycles of sufficient sediment resupply to reaches of sufficient transport capacity in a single year suggest an intermediate regime with frequent switches between periods with sediment- and transport limitation. In contrast, debris flows are strongly coupled to the timing of wet conditions in the moderately steep ID3 (~18° in the source area), with both largely occurring within a rather concentrated period in late summer (Figure 8). In other words, as debris flows occur mostly during periods of extreme wetness conditions, this suggests that under less-than-extreme conditions, the in-stream transport capacity is insufficient to trigger debris flows despite potentially sufficient available sediment. The strong coupling

https://doi.org/10.5194/egusphere-2026-5589
Preprint. Discussion started: 24 September 2026

in ID3 can therefore be interpreted as evidence for a transport limited debris flow regime. As an expression of geomorphic predisposition that describes the physical features of the landscape, including topography, geology or soil types, the above implies that seasonal debris flow regimes can exhibit major differences even at very local scales, and thus between catchments in close geographical proximity and with similar climatic predisposition.

6.2 Implications for regional threshold models

A major implicit assumption and weakness of regional thresholds is that debris flows over the spatial model domain are characterized by similar climatic and geomorphic predispositions and are triggered by the same mechanism and thus belong to the same distribution. The above-described differences in debris flow regimes however clearly illustrate that individual channels can characterized by unique combinations of climatic predisposition, geomorphic predisposition and hydro-meteorological trigger conditions even over small distances.
Although, the performance of regional thresholds in our analysis is rather robust and similar to other studies (e.g. Jiang et al., 2021; Moreno et al., 2025), they are consistently and in part considerably outperformed by local thresholds across all study channels (Figure 13). It is, of course, not unexpected that locally fitted thresholds are stronger descriptors of local conditions than regional thresholds. For example, Bel et al. (2017) and Nikolopoulos et al. (2015) showed that thresholds in the French Prealps and Trento-Alto Adige region of Italy, respectively, are subject to pronounced spatial differences when discretizing the spatial domain into smaller sub-regions. Going beyond that, our results in addition specifically reveal that regional thresholds can be too conservative and can lead to unnecessarily inflated false positive rates. This is of relevance when such regional thresholds are used as operational early warning system, as such elevated rates of false alarms may eventually undermine the credibility of and trust in issued debris flow warnings. As a step forward towards more robust and general regional models, it will be necessary to move away from bi-variate thresholds towards higher dimensional models based on multivariate thresholds, to better capture spatial contrasts in hydro-meteorological triggers (e.g. Bel et al., 2017) as well as in climatic (e.g. Prenner et al., 2018) and geomorphic predisposition, as recently demonstrated by Moreno et al. (2025).

6.3 Value of liquid water input and stream flow for thresholds models

The use of precipitation P or rainfall P_R for the development of thresholds instead of explicit consideration of liquid water input as the combination of rain and snow melt as $P_L = P_R + P_M$, can mask the subtleties of underlying processes in different ways. On the one hand, such a threshold will fail to detect debris flows that are exclusively triggered by snow melt $P_M > 0$ mm hr^{-1} at moments with no further rainfall ($P_R = 0$ mm hr^{-1}) as observed in ID 2 (Figure 10a,b) and may thus enhance false negative rates (Figure 13b). On the other hand, it can lead to elevated levels of false positives (Figure 13a,c), by overestimating event intensities and underestimating event durations, as rainfall events are overall characterized by higher intensities and shorter durations than snowmelt events. The benefit of developing thresholds based on P_L is evident in their systematically and in part substantially higher performances than P and P_R based thresholds in all three study channels both at local and regional scales (Figure 13d-i).

https://doi.org/10.5194/egusphere-2026-5589
Preprint. Discussion started: 24 September 2026

However, any variable of water input, i.e. P, P_R or P_L, remains a rough proxy to describe in-stream transport capacity, i.e. discharge Q. In reality, the subsurface acts as a non-linear low-pass filter that regulates the release of water to the channel based on its wetness state (e.g. soil moisture, groundwater level), which is a result of the past sequence of water input and output. The resulting non-unique relationship between water input and discharge Q then entails that the same magnitudes of water input can, depending on the wetness state, lead to substantial differences in Q. The role of Q as a more direct and meaningful descriptor of in-stream transport capacity, is underlined by the fact that local thresholds based on Q exhibit the consistently highest performances across all study channels (Figure 13). Notably, due to the continuous nature of discharge and time lags between water input and discharge peaks, thresholds defined on basis of Q can even detect debris flows that occur at moments when $P_L = 0$ mm hr^{-1} (Figure 10e,f). While local thresholds based on Q systematically outperform all other thresholds, the value of discharge as predictor is more ambiguous for regional thresholds (Figure 13d-i). As the hydrological response as expressed by Q is a manifestation of local catchment characteristics, and thus also of geomorphic predisposition, differences in catchment characteristics inevitably lead to differences in how water is stored and released as Q in different catchments, making spatial generalization a problematic and so far largely unresolved issue (e.g. Rudlang et al., 2026).

6.4 Uncertainties and limitations

Although the role of snowmelt and discharge as predictors for debris flow is evident from the above results, as also similarly reported by a few other studies (Mostbauer et al., 2018; Bernard et al., 2025), it is only rarely considered in threshold models. The main reason clearly being the lack of discharge or at least stream water level observations in mountain channels of low stream order. Without these observations, the calibration of hydrological model and their subsequent use for discharge predictions remains a considerable challenge. In addition, in channels where such observations are available, predictions of discharge Q and other variables such as snow melt P_M or soil moisture S_U can be subject to considerable uncertainties due to uncertainties in input data, including precipitation, model architecture as well as the choice of model parameters (e.g. Beven, 2024). As can be seen in Figures 4 and 6, the uncertainty bounds of the shown modelled variables in this study can be rather wide. However, and encouragingly, the effects of these uncertainties – shown as error bars in Figures 8-11 – on the debris flow thresholds are very limited and do not change the importance of, in particular, P_L and Q as modelled debris flow predictors across the three study catchments (Figure 13). Notwithstanding the availability of complete and long timeseries of discharge observations, recent research has suggested that already the availability of intermittent, anecdotal estimates of discharge at a few moments (Pool and Seibert, 2021) or estimates of indicative water-level class (Clerc-Schwarzenbach et al., 2025), in particular when combined with remotely sensed snow cover information (Tong et al., 2021; Khalil et al., 2026) may be sufficient for robust model parameter estimates. As also demonstrated by the results of our analysis, such approaches based on anecdotal and/or indicative data may offer a feasible way to calibrate models and eventually predict variables such as P_L and Q in debris flow-prone channels in which it may otherwise be logistically challenging to systematically monitor stream flow over long time periods.

https://doi.org/10.5194/egusphere-2026-5589
Preprint. Discussion started: 24 September 2026

7 Conclusions

In this study we have analysed long-term records of debris flows, hydro-meteorological and modelled hydrological variables for three contrasting active debris flow channels (ID1, ID2 and ID3) in the Austrian Alps, extending over periods of up to 18 years.

We have found that:

(1) the three channels are characterized by distinct seasonal timing of debris flow events. Debris flows in ID1 concentrate in early summer and, on average, occur several weeks before the wettest conditions in individual years. This weak temporal coupling between debris flows and hydro-meteorological conditions suggests insufficient sediment resupply to trigger debris flows in spite of sufficient in-stream transport capacity in late summer. ID2 is characterized by debris flows that are spread throughout summer, occurring on average a few days after the wettest annual conditions. This moderate temporal coupling is a fingerprint of multiple cycles of sediment resupply and sediment exhaustion with sufficient transport capacity available throughout summer. In contrast, debris flows in ID3 are strongly coupled to hydro-meteorological conditions. They occur mostly late in summer and coincide with the wettest annual conditions, suggesting that only these extreme wetness conditions provide sufficient transport capacity to trigger debris flows. While the distinct debris flow pattern between ID1/ ID2 and ID3 illustrate the importance of spatial differences in hydro-climatic conditions, the differences between the geographically close channels ID1 and ID2 are largely a result of differences in landscape and geomorphological characteristics. Together these differences illustrate that even over short distances, debris flows can be subject to highly contrasting regimes with distinct underlying processes.

(2) As a result of these different regimes and the associated distinct hydro-climatic and geomorphic predisposition of the study channels, regional debris flow thresholds, even over short distances, can be markedly too conservative. Depending on the channel, they can cause inflated rates of false negatives (missed debris flows) or of false positives (false alarms). Overall, local thresholds outperform regional thresholds across the study catchments.

(3) Explicitly accounting for the precipitation phase and thus the effect of liquid precipitation, estimated as combined rainfall and snow melt, i.e. $P_L = P_R + P_M$, systematically outperforms precipitation P and rainfall P_R, for both, regional and local debris flow thresholds. For local thresholds, the combination of discharge Q with the intensity of P_L was found to be the strongest predictor across all study channels, underlining the critical role of discharge as descriptor of in-stream transport capacity for prediction of debris flows.

Overall, the results of this study illustrate the importance of spatial heterogeneity in climatic and geomorphic predisposition, leading to distinct debris flow regimes that are controlled by different underlying processes. It was further demonstrated that relatively little additional information, such as remotely sensed snow cover data or anecdotal stream flow observations, can prove highly valuable to estimate P_L and with some more effort Q, which are consistently and considerably stronger predictors of debris flows than traditionally used precipitation or rainfall.

Author contribution. MH and RK conceptualized the study. RK coordinated and executed the field monitoring campaign. MH carried out the analysis with input from RK. MH wrote the manuscript collaboration with RK.

Code and data availability. Raw hydro-meteorological data can be requested from GeoSphere Austria. Pre-processed hydro-meteorological, hydrological and debris flow data as well as the code of the hydrological model are available at online via the 4TU data repository at https://data.4tu.nl/jGRwbb9Vwsup1UuzFoQt1QedU_JMcjsp0jvBijeRTS4

Competing interests. One of the authors is a member of the editorial board of Hydrology and Earth System Sciences.

Acknowledgements. We are grateful to Philipp Aigner und Urban Aichner for collecting field data and the Austrian Forest Service for Torrent and Avalanche Control for supporting debris flow monitoring at Lattenbach catchment. Microsoft Copilot was used for language editing of the title of this article.

Financial support. This project was funded by the Austrian Climate Research Programme, project no. B960253, ACRP11 - Deucalion III - KR18AC0K14670

References

Aigner, P., Kuschel, E., Sklar, L., Zangerl, C., Hrachowitz, M., De Haas, T., et al. (2023). Debris-flow activity and sediment dynamics in the landslide-influenced Lattenbach catchment, Austria. In E3S Web of Conferences (Vol. 415, p. 04001). Torino. https://doi.org/10.1051/e3sconf/202341504001

Astagneau, P. C., Wood, R. R., & Brunner, M. I. (2026). Rethinking future flood hazard: Hourly data challenge daily flood projections in Alpine catchments. *Science Advances*, *12*(29), eaed6012. https://doi.org/10.1126/sciadv.aed6012

Bel, C., Liébault, F., Navratil, O., Eckert, N., Bellot, H., Fontaine, F., & Laigle, D. (2017). Rainfall control of debris-flow triggering in the Réal Torrent, Southern French Prealps. Geomorphology, 291, 17-32. https://doi.org/10.1016/j.geomorph.2016.04.004

Bennett, G. L., Molnar, P., McArdell, B. W., & Burlando, P. (2014). A probabilistic sediment cascade model of sediment transfer in the Illgraben. Water Resources Research, 50(2), 1225–1244. https://doi.org/10.1002/2013WR013806

Bernard, M., Barbini, M., Berti, M., Boreggio, M., Simoni, A., & Gregoretti, C. (2025). Rainfall-runoff modeling in rocky headwater catchments for the prediction of debris flow occurrence. Water Resources Research, 61(1), e2023WR036887. https://doi.org/10.1029/2023WR036887

Bernardi, T.C. (2022). Assessment of movement rates and sediment dynamics at Loechertroggraben - Defereggen valley, Austria. Master thesis, BOKU University. https://permalink.obvsg.at/bok/AC16746924

https://doi.org/10.5194/egusphere-2026-5589
Preprint. Discussion started: 24 September 2026

Berti, M., Martina, M. L. V., Franceschini, S., Pignone, S., Simoni, A., & Pizziolo, M. (2012). Probabilistic rainfall thresholds for landslide occurrence using a Bayesian approach. Journal of Geophysical Research: Earth Surface, 117(F4). https://doi.org/10.1029/2012JF002367

Beven, K. (2024). A brief history of information and disinformation in hydrological data and the impact on the evaluation of hydrological models. Hydrological Sciences Journal, 69(5), 519-527. https://doi.org/10.1080/02626667.2024.2332616

BMLUK (2026). Wildbach- und Lawinenkataster, available at https://geoportal.inspire.gv.at

Bogaard, T., & Greco, R. (2018). Invited perspectives: Hydrological perspectives on precipitation intensity-duration thresholds for landslide initiation: proposing hydro-meteorological thresholds. Natural Hazards and Earth System Sciences, 18(1), 31-39. https://doi.org/10.5194/nhess-18-31-2018

Borga, M., Vezzani, C., & Fontana, G. D. (2005). Regional rainfall depth–duration–frequency equations for an alpine region. Natural Hazards, 36(1), 221-235. https://doi.org/10.1007/s11069-004-4550-y

Bouaziz, L. J., Aalbers, E. E., Weerts, A. H., Hegnauer, M., Buiteveld, H., Lammersen, R., ... & Hrachowitz, M. (2022). Ecosystem adaptation to climate change: the sensitivity of hydrological predictions to time-dynamic model parameters. Hydrology and Earth System Sciences, 26(5), 1295-1318. https://doi.org/10.5194/hess-26-1295-2022

Bovis, M. J., & Jakob, M. (1999). The role of debris supply conditions in predicting debris flow activity. *Earth Surface Processes and Landforms*, *24*(11), 1039–1054. https://doi.org/10.1002/(SICI)1096-9837(199910)24:11%3C1039::AID-ESP29%3E3.0.CO;2-U

Brenna, A., Surian, N., Ghinassi, M., & Marchi, L. (2020). Sediment–water flows in mountain streams: Recognition and classification based on field evidence. Geomorphology, 371, 107413. https://doi.org/10.1016/j.geomorph.2020.107413

Caine, N. (1980). The rainfall intensity-duration control of shallow landslides and debris flows. Geografiska Annaler: Series A, Physical Geography, 62, 23-27. https://doi.org/10.1080/04353676.1980.11879996

Clerc-Schwarzenbach, F., Seibert, J., Vis, M., & van Meerveld, I. (2025). Value of water level class observations for parameter set selection in hydrological modelling. Hydrological Sciences Journal, 70(9), 1464-1480. https://doi.org/10.1080/02626667.2025.2489994

Destro, E., Marra, F., Nikolopoulos, E. I., Zoccatelli, D., Creutin, J. D., & Borga, M. (2017). Spatial estimation of debris flows-triggering rainfall and its dependence on rainfall return period. Geomorphology, 278, 269-279. https://doi.org/10.1016/j.geomorph.2016.11.019

Dowling, C. A., & Santi, P. M. (2014). Debris flows and their toll on human life: a global analysis of debris-flow fatalities from 1950 to 2011. Natural Hazards, 71(1), 203–227. https://doi.org/10.1007/s11069-013-0907-4

Efstratiadis, A., & Koutsoyiannis, D. (2010). One decade of multi-objective calibration approaches in hydrological modelling: a review. Hydrological Sciences Journal, 55(1), 58-78. https://doi.org/10.1080/02626660903526292

Euser, T., Hrachowitz, M., Winsemius, H. C., & Savenije, H. H. (2015). The effect of forcing and landscape distribution on performance and consistency of model structures. Hydrological processes, 29(17), 3727-3743. https://doi.org/10.1002/hyp.10445

https://doi.org/10.5194/egusphere-2026-5589
Preprint. Discussion started: 24 September 2026

Freer, J., Beven, K., & Ambroise, B. (1996). Bayesian estimation of uncertainty in runoff prediction and the value of data: An application of the GLUE approach. Water resources research, 32(7), 2161-2173. https://doi.org/10.1029/95WR03723

Gao, H., Hrachowitz, M., Sriwongsitanon, N., Fenicia, F., Gharari, S., & Savenije, H. H. (2016). Accounting for the influence of vegetation and landscape improves model transferability in a tropical savannah region. Water Resources Research, 52(10), 7999-8022. https://doi.org/10.1002/2016WR019574

Gregoretti, C., & Fontana, G. D. (2008). The triggering of debris flow due to channel-bed failure in some alpine headwater basins of the Dolomites: Analyses of critical runoff. Hydrological Processes, 22(13), 2248-2263. https://doi.org/10.1002/hyp.6821

Gregoretti, C., Degetto, M., Bernard, M., Crucil, G., Pimazzoni, A., De Vido, G., et al. (2016). Runoff of small rocky headwater catchments: Field observations and hydrological modeling. Water Resources Research, 52(10), 8138–8158. https://doi.org/10.1002/2016wr018675

Gupta, H. V., Wagener, T., & Liu, Y. (2008). Reconciling theory with observations: elements of a diagnostic approach to model evaluation. Hydrological Processes, 22(18), 3802-3813. https://doi.org/10.1002/hyp.6989

Guzzetti, F., Peruccacci, S., Rossi, M., & Stark, C. P. (2008). The rainfall intensity–duration control of shallow landslides and debris flows: an update. Landslides, 5(1), 3-17. https://doi.org/10.1007/s10346-007-0112-1

Hall, D.K., Riggs, G.A.: MODIS/Terra Snow Cover Daily L3 Global 500m Grid, Version 6. Boulder, Colorado USA. NASA National Snow and Ice Data Center Distributed Active Archive Center. https://doi.org/10.5067/MODIS/MOD10A1.006.

Haslinger, K., Breinl, K., Pavlin, L., Pistotnik, G., Bertola, M., Olefs, M., et al. (2025). Increasing hourly heavy rainfall in Austria reflected in flood changes. Nature, 639(8055), 667–672. https://doi.org/10.1038/s41586-025-08647-2

Hanus, S., Hrachowitz, M., Zekollari, H., Schoups, G., Vizcaino, M., & Kaitna, R. (2021). Future changes in annual, seasonal and monthly runoff signatures in contrasting Alpine catchments in Austria. Hydrology and Earth System Sciences, 25(6), 3429-3453. https://doi.org/10.5194/hess-25-3429-2021

Hargreaves, G. H., & Samani, Z. A. (1982). Estimating potential evapotranspiration. Journal of the irrigation and Drainage Division, 108(3), 225-230. https://doi.org/10.1061/JRCEA4.0001390

Hirschberg, J., Fatichi, S., Bennett, G. L., McArdell, B. W., Peleg, N., Lane, S. N., et al. (2021). Climate Change Impacts on Sediment Yield and Debris-Flow Activity in an Alpine Catchment. *Journal of Geophysical Research: Earth Surface*, *126*(1), e2020JF005739. https://doi.org/10.1029/2020JF005739

Hirschberg, J., McArdell, B. W., Bennett, G. L., & Molnar, P. (2022). Numerical Investigation of Sediment-Yield Underestimation in Supply-Limited Mountain Basins With Short Records. *Geophysical Research Letters*, *49*(7), e2021GL096440. https://doi.org/10.1029/2021GL096440

Hrachowitz, M., Fovet, O., Ruiz, L., Euser, T., Gharari, S., Nijzink, R., ... & Gascuel-Odoux, C. (2014). Process consistency in models: The importance of system signatures, expert knowledge, and process complexity. Water resources research, 50(9), 7445-7469. https://doi.org/10.1002/2014WR015484

https://doi.org/10.5194/egusphere-2026-5589
Preprint. Discussion started: 24 September 2026

Hrachowitz, M., Stockinger, M., Coenders-Gerrits, M., van der Ent, R., Bogena, H., Lücke, A., & Stumpp, C. (2021). Reduction of vegetation-accessible water storage capacity after deforestation affects catchment travel time distributions and increases young water fractions in a headwater catchment. Hydrology and Earth System Sciences, 25(9), 4887-4915. https://doi.org/10.5194/hess-25-4887-2021

Huebl, J., & Kaitna, R. (2021). Monitoring Debris-Flow Surges and Triggering Rainfall at the Lattenbach Creek, Austria. Environmental and Engineering Geoscience, 27(2), 213–220. https://doi.org/10.2113/EEG-D-20-00010

Hulsman, P., Hrachowitz, M., & Savenije, H. H. (2021). Improving the representation of long-term storage variations with conceptual hydrological models in data-scarce regions. Water Resources Research, 57(4), e2020WR028837. https://doi.org/10.1029/2020WR028837

Hungr, O., Leroueil, S., & Picarelli, L. (2014). The Varnes classification of landslide types, an update. Landslides, 11(2), 167-194. https://doi.org/10.1007/s10346-013-0436-y

Jakob, M., Owen, T., & Simpson, T. (2012). A regional real-time debris-flow warning system for the District of North Vancouver, Canada. Landslides, 9(2), 165-178. https://doi.org/10.1007/s10346-011-0282-8

Jiang, Z., Fan, X., Subramanian, S. S., Yang, F., Tang, R., Xu, Q., & Huang, R. (2021). Probabilistic rainfall thresholds for debris flows occurred after the Wenchuan earthquake using a Bayesian technique. Engineering Geology, 280, 105965.l geography, 62(1-2), 23-27. https://doi.org/10.1016/j.enggeo.2020.105965

Kaitna, R., Prenner, D., Switanek, M., Maraun, D., Stoffel, M., & Hrachowitz, M. (2023a). Changes of hydro-meteorological trigger conditions for debris flows in a future alpine climate. Science of the Total Environment, 872, 162227. https://doi.org/10.1016/j.scitotenv.2023.162227

Kaitna, R., Aigner, P., Bernardi, T., Wagner, P., Kuschel, E., Zangerl, C., Hrachowitz, M., and Sklar, L. (2023b). Sediment dynamics related to the triggering of debris flows in different alpine watersheds, EGU General Assembly 2023, Vienna, Austria, 24–28 Apr 2023, EGU23-8751. https://doi.org/10.5194/egusphere-egu23-8751

Kaitna, R., Schlögl, M., Becsi, B., Rieder, H., & Formayer, H. (2025). Climate induced increase in frequency and area affected by critical rainfall conditions triggering debris flows in Austria. Communications Earth & Environment, 6(1), 793. https://doi.org/10.1038/s43247-025-02760-w

Kean, J. W., McCoy, S. W., Tucker, G. E., Staley, D. M., & Coe, J. A. (2013). Runoff-generated debris flows: Observations and modeling of surge initiation, magnitude, and frequency. Journal of Geophysical Research: Earth Surface, 118(4), 2190-2207. https://doi.org/10.1002/jgrf.20148

Khalil, A., Tong, R., Majid, Z., Széles, B., Bertola, M., & Parajka, J. (2026). Multiple-objective calibration of a conceptual hydrological model using satellite data of snow cover, soil moisture and limited streamflow observations. EGUsphere, 2026, 1-30. https://doi.org/10.5194/egusphere-2026-2880

Leonarduzzi, E., Molnar, P., & McArdell, B. W. (2017). Predictive performance of rainfall thresholds for shallow landslides in Switzerland from gridded daily data. Water Resources Research, 53(8), 6612-6625. https://doi.org/10.1002/2017WR021044

Long, K., Zhang, S., Wei, F., Hu, K., Zhang, Q., & Luo, Y. (2020). A hydrology-process based method for correlating debris flow density to rainfall parameters and its application on debris flow prediction. Journal of hydrology, 589, 125124. https://doi.org/10.1016/j.jhydrol.2020.125124

Marra, F. (2019). Rainfall thresholds for landslide occurrence: systematic underestimation using coarse temporal resolution data. Natural Hazards, 95(3), 883-890. https://doi.org/10.1007/s11069-018-3508-4

Marra, F., Destro, E., Nikolopoulos, E. I., Zoccatelli, D., Creutin, J. D., Guzzetti, F., & Borga, M. (2017). Impact of rainfall spatial aggregation on the identification of debris flow occurrence thresholds. Hydrology and Earth System Sciences, 21(9), 4525-4532. https://doi.org/10.5194/hess-21-4525-2017

Marra, F., Dallan, E., Borga, M., Greco, R., & Bogaard, T. (2025). Brief communication: Threshold and probability. The conceptual difference between ID thresholds for landslide initiation and IDF curves. Natural Hazards and Earth System Sciences, 25(12), 5055-5061. https://doi.org/10.5194/nhess-25-5055-2025

McGuire, L. A., Rengers, F. K., Kean, J. W., & Staley, D. M. (2017). Debris flow initiation by runoff in a recently burned basin: Is grain-by-grain sediment bulking or en masse failure to blame? Geophysical Research Letters, 44(14), 7310–7319. https://doi.org/10.1002/2017GL074243

Meyer, N. K., Dyrrdal, A. V., Frauenfelder, R., Etzelmüller, B., & Nadim, F. (2012). Hydrometeorological threshold conditions for debris flow initiation in Norway. Natural Hazards and Earth System Sciences, 12(10), 3059-3073. https://doi.org/10.5194/nhess-12-3059-2012

Mirus, B. B., Bogaard, T., Greco, R., & Stähli, M. (2025). Invited perspectives: Integrating hydrologic information into the next generation of landslide early warning systems. Natural Hazards and Earth System Sciences, 25(1), 169-182. https://doi.org/10.5194/nhess-25-169-2025

Montgomery, D. R., & Buffington, J. M. (1997). Channel-reach morphology in mountain drainage basins. Geological Society of America Bulletin, 109(5), 596-611. https://doi.org/10.1130/0016-7606(1997)109%3C0596:CRMIMD%3E2.3.CO;2

Moreno, M., Lombardo, L., Steger, S., de Vugt, L., Zieher, T., Crespi, A., ... & Opitz, T. (2025). Functional regression for space-time prediction of precipitation-induced shallow landslides in South Tyrol, Italy. Journal of Geophysical Research: Earth Surface, 130(4), e2024JF008219. https://doi.org/10.1029/2024JF008219

Mostbauer, K., Kaitna, R., Prenner, D., & Hrachowitz, M. (2018). The temporally varying roles of rainfall, snowmelt and soil moisture for debris flow initiation in a snow-dominated system. Hydrology and Earth System Sciences, 22(6), 3493-3513. https://doi.org/10.5194/hess-22-3493-2018

Nijzink, R. C., Samaniego, L., Mai, J., Kumar, R., Thober, S., Zink, M., ... & Hrachowitz, M. (2016). The importance of topography-controlled sub-grid process heterogeneity and semi-quantitative prior constraints in distributed hydrological models. Hydrology and Earth System Sciences, 20(3), 1151-1176. https://doi.org/10.5194/hess-20-1151-2016

Nikolopoulos, E. I., Borga, M., Marra, F., Crema, S., & Marchi, L. (2015). Debris flows in the eastern Italian Alps: seasonality and atmospheric circulation patterns. Natural Hazards and Earth System Science, 15(3), 647-656. https://doi.org/10.5194/nhess-15-647-2015

https://doi.org/10.5194/egusphere-2026-5589
Preprint. Discussion started: 24 September 2026

Palucis, M. C., Ulizio, T., Fuller, B., & Lamb, M. P. (2018). Intense Granular Sheetflow in Steep Streams. *Geophysical Research Letters*, *45*(11), 5509–5517. https://doi.org/10.1029/2018GL077526

Parajka, J., & Blöschl, G. (2008). The value of MODIS snow cover data in validating and calibrating conceptual hydrologic models. Journal of hydrology, 358(3-4), 240-258. https://doi.org/10.1016/j.jhydrol.2008.06.006

Ponds, M., Hanus, S., Zekollari, H., ten Veldhuis, M. C., Schoups, G., Kaitna, R., & Hrachowitz, M. (2025). Adaptation of root zone storage capacity to climate change and its effects on future streamflow in Alpine catchments: towards non-stationary model parameters. Hydrology and Earth System Sciences, 29(15), 3545-3568. https://doi.org/10.5194/hess-29-3545-2025

Pool, S., & Seibert, J. (2021). Gauging ungauged catchments–Active learning for the timing of point discharge observations in combination with continuous water level measurements. Journal of Hydrology, 598, 126448. https://doi.org/10.1016/j.jhydrol.2021.126448

Prenner, D., Kaitna, R., Mostbauer, K., & Hrachowitz, M. (2018). The value of using multiple hydrometeorological variables to predict temporal debris flow susceptibility in an alpine environment. Water Resources Research, 54(9), 6822-6843. https://doi.org/10.1029/2018WR022985

Prenner, D., Hrachowitz, M., & Kaitna, R. (2019). Trigger characteristics of torrential flows from high to low alpine regions in Austria. Science of the Total Environment, 658, 958-972. https://doi.org/10.1016/j.scitotenv.2018.12.206

Rudlang, J. M., do Nascimento, T. V., van der Ent, R., Fenicia, F., & Hrachowitz, M. (2026). Climate and landscape jointly control European streamflow behaviour. Hydrology and Earth System Sciences, 30. https://doi.org/10.5194/hess-30-4481-2026

Qie, J., Favillier, A., Liébault, F., Ballesteros Cánovas, J. A., Lopez-Saez, J., Guillet, S., et al. (2024). A supply-limited torrent that does not feel the heat of climate change. *Nature Communications*, *15*(1), 9078. https://doi.org/10.1038/s41467-024-53316-z

Schoups, G., Hopmans, J. W., Young, C. A., Vrugt, J. A., & Wallender, W. W. (2005). Multi-criteria optimization of a regional spatially-distributed subsurface water flow model. Journal of Hydrology, 311(1-4), 20-48. https://doi.org/10.1016/j.jhydrol.2005.01.001

Takahashi, T. (1978). Mechanical characteristics of debris flow. *Journal of the Hydraulics Division*, *104*(8), 1153–1169. https://doi.org/10.1061/JYCEAJ.0005046

Tempel, N., Bouaziz, L., Taormina, R., van Noppen, E., Stam, J., Sprokkereef, E., & Hrachowitz, M. (2024). Catchment response to climatic variability: implications for root zone storage and streamflow predictions. Hydrology and Earth System Sciences, 28(20), 4577-4597. https://doi.org/10.5194/hess-28-4577-2024

Tong, R., Parajka, J., Komma, J., & Blöschl, G. (2020). Mapping snow cover from daily Collection 6 MODIS products over Austria. Journal of Hydrology, 590, 125548. https://doi.org/10.1016/j.jhydrol.2020.125548

Tong, R., Parajka, J., Salentinig, A., Pfeil, I., Komma, J., Széles, B., ... & Blöschl, G. (2021). The value of ASCAT soil moisture and MODIS snow cover data for calibrating a conceptual hydrologic model. Hydrology and Earth System Sciences, 25(3), 1389-1410. https://doi.org/10.5194/hess-25-1389-2021

Wagner, P. (2022). Analyse der Sedimentdynamik im Wildbach Hopfgartnergraben auf Basis digitaler Fernerkundung und Photogrammetrie. Master thesis, BOKU University. https://epub.boku.ac.at/urn/urn:nbn:at:at-ubbw:1-43747

Wang, S., Hrachowitz, M., & Schoups, G. (2024). Multi-decadal fluctuations in root zone storage capacity through vegetation adaptation to hydro-climatic variability have minor effects on the hydrological response in the Neckar River basin, Germany. Hydrology and Earth System Sciences, 28(17), 4011-4033. https://doi.org/10.5194/hess-28-4011-2024

Wei, Z., Shang, Y., Zhao, Y., Pan, P., & Jiang, Y. (2017). Rainfall threshold for initiation of channelized debris flows in a small catchment based on in-site measurement. Engineering Geology, 217, 23-34. https://doi.org10.1016/j.enggeo.2016.12.003

Zhuang, J., Cui, P., Wang, G., Chen, X., Iqbal, J., & Guo, X. (2015). Rainfall thresholds for the occurrence of debris flows in the Jiangjia Gully, Yunnan Province, China. Engineering Geology, 195, 335-346. https://doi.org/10.1016/j.enggeo.2015.06.006